ARTICLE

Bi-allelic mutations of *DNAH10* cause primary male infertility with asthenoteratozoospermia in humans and mice

Chaofeng Tu,[1,2,10] Jiangshan Cong,[3,4,10] Qianjun Zhang,[1,2,10] Xiaojin He,[5,6,7,10] Rui Zheng,[8,10] Xiaoxuan Yang,[1] Yang Gao,[5,6,7] Huan Wu,[5,6,7] Mingrong Lv,[5,6,7] Yayun Gu,[9] Shuai Lu,[9] Chunyu Liu,[3,4] Shixiong Tian,[3,4] Lanlan Meng,[2] Weili Wang,[1] Chen Tan,[1] Hongchuan Nie,[2] Dongyan Li,[1] Huan Zhang,[2] Fei Gong,[1,2] Liang Hu,[1,2] Guangxiu Lu,[2] Wenming Xu,[8,11] Ge Lin,[1,2,11] Feng Zhang,[3,4,11] Yunxia Cao,[5,6,7,11,*] and Yue-Qiu Tan[1,2,11,*]

Summary

Multiple morphological abnormalities of the sperm flagella (MMAF)-induced asthenoteratozoospermia is a common cause of male infertility. Previous studies have identified several MMAF-associated genes, highlighting the condition's genetic heterogeneity. To further define the genetic causes underlying MMAF, we performed whole-exome sequencing in a cohort of 643 Chinese MMAF-affected men. Bi-allelic *DNAH10* variants were identified in five individuals with MMAF from four unrelated families. These variants were either rare or absent in public population genome databases and were predicted to be deleterious by multiple bioinformatics tools. Morphological and ultrastructural analyses of the spermatozoa obtained from men harboring bi-allelic *DNAH10* variants revealed striking flagellar defects with the absence of inner dynein arms (IDAs). *DNAH10* encodes an axonemal IDA heavy chain component that is predominantly expressed in the testes. Immunostaining analysis indicated that DNAH10 localized to the entire sperm flagellum of control spermatozoa. In contrast, spermatozoa from the men harboring bi-allelic *DNAH10* variants exhibited an absence or markedly reduced staining intensity of DNAH10 and other IDA components, including DNAH2 and DNAH6. Furthermore, the phenotypes were recapitulated in mouse models lacking *Dnah10* or expressing a disease-associated variant, confirming the involvement of DNAH10 in human MMAF. Altogether, our findings in humans and mice demonstrate that DNAH10 is essential for sperm flagellar assembly and that deleterious bi-allelic *DNAH10* variants can cause male infertility with MMAF. These findings will provide guidance for genetic counseling and insights into the diagnosis of MMAF-associated asthenoteratozoospermia.

Introduction

Male infertility is a major reproductive disorder characterized by a complex multifactorial pathogenesis with a highly heterogeneous clinical phenotype of abnormal sperm count and/or quality.[1,2] Asthenoteratozoospermia, defined by the decrease of motile sperm with morphological abnormality in ejaculation, is one of the main clinical presentations of male infertility.[3] Multiple morphological abnormalities of the flagella (MMAF) is a severe form of asthenoteratozoospermia and is characterized by the presence of immotile spermatozoa presenting severe flagellar malformations (e.g., absent, coiled, short, bent, and/or irregular-caliber flagella).[4] An increasing number of studies have explored the genetic etiology of MMAF, suggesting that MMAF is a disorder of highly heterogeneous genetic origin.[5,6] To date, 24 MMAF-associated genes have been reported to be responsible for the occurrence of primary infertility without the manifestation of any symptoms of primary ciliary dyskinesia (PCD [MIM: 244400]), for example, recurrent respiratory infections and left-right laterality disturbances.[7–10] However, these findings are reported in approximately 60% of the MMAF-affected individuals, indicating the potential involvement of other genetic factors in asthenoteratozoospermia.

Flagella and cilia are hair-like microtubule-based structures that share an important core component: the axoneme.[11] It is a highly ordered 9 + 2 arrangement of nine doublets of microtubules (A and B) and a central pair of microtubules, exhibiting evolutionary conservation from protozoa to humans.[12,13] Axonemal dynein arms, consisting of outer and inner dynein arms (ODAs and IDAs, respectively), are attached to the A-microtubule of each peripheral

[1]Institute of Reproductive and Stem Cell Engineering, School of Basic Medical Science, Central South University, Changsha 410000, China; [2]Clinical Research Center for Reproduction and Genetics in Hunan Province, Reproductive and Genetic Hospital of CITIC-Xiangya, Changsha 410000, China; [3]Obstetrics and Gynecology Hospital, NHC Key Laboratory of Reproduction Regulation (Shanghai Institute for Biomedical and Pharmaceutical Technologies), State Key Laboratory of Genetic Engineering at School of Life Sciences, Fudan University, Shanghai 200011, China; [4]Shanghai Key Laboratory of Female Reproductive Endocrine Related Diseases, Shanghai 200011, China; [5]Reproductive Medicine Center, Department of Obstetrics and Gynecology, The First Affiliated Hospital of Anhui Medical University, Hefei 230022, China; [6]NHC Key Laboratory of Study on Abnormal Gametes and Reproductive Tract, Anhui Medical University, Hefei 230032, China; [7]Key Laboratory of Population Health Across Life Cycle, Anhui Medical University, Ministry of Education of the People's Republic of China, Hefei 230032, China; [8]Department of Obstetrics/Gynecology, Key Laboratory of Obstetric, Gynecologic and Pediatric Diseases and Birth Defects of Ministry of Education, West China Second University Hospital, Sichuan University, Chengdu 610041, China; [9]State Key Laboratory of Reproductive Medicine, Center for Global Health, School of Public Health, Nanjing Medical University, Nanjing 211166, China
[10]These authors contributed equally
[11]Senior author
*Correspondence: caoyunxia6@126.com (Y.C.), tanyueqiu@csu.edu.cn (Y.-Q.T.)
https://doi.org/10.1016/j.ajhg.2021.06.010.

doublet.[14] IDAs and ODAs are multiprotein ATPase complexes, which are composed of light, intermediate, and heavy chain proteins that hydrolyze ATP for ciliary and flagellar beating.[15,16] There are 13 dynein axonemal heavy chain (DNAH) proteins (DNAH1–3, DNAH5–12, DNAH14, and DNAH17) in humans.[17] In previous studies, mutations in two IDA heavy-chain-protein-encoding genes, *DNAH1* (MIM: 603332) and *DNAH2* (MIM: 603333), and two ODA heavy chain components, *DNAH8* (MIM: 603337) and *DNAH17* (MIM: 610063), have been described in individuals with isolated male infertility occurring because of asthenoteratozoospermia.[4,8,18,19] These findings suggest that mutations in other heavy chain components may be an underlying cause of male infertility with sperm flagellar malformations. Interestingly, *DNAH10* (MIM: 605884), encoding an IDA heavy chain protein, exhibits testis-specific mRNA expression in humans, but its functional role in male fertility has not been characterized thus far.

In this study, we identified bi-allelic variants of *DNAH10* in five men with asthenoteratozoospermia from four unrelated families. Furthermore, *Dnah10*-knockout male mice and *Dnah10*-knockin male mice harboring a homozygous missense variant ($Dnah10^{M/M}$) equivalent to that observed in one individual (T012 II-2, c.12838G>A) were generated with the CRISPR-Cas9 technology. The mutant adult males were sterile and presented a typical MMAF phenotype, including complete sperm immobility and abnormal flagellar morphology. Taken together, these findings strongly suggest that bi-allelic variants of *DNAH10* can induce MMAF-associated asthenoteratozoospermia in humans and mice.

Material and methods

Human subjects

A cohort of 643 MMAF-affected Chinese men was recruited from the Reproductive and Genetic Hospital of CITIC-Xiangya (Changsha, China) and the First Affiliated Hospital of Anhui Medical University (Hefei, China). The clinical phenotypes of the affected individuals are described in the supplemental information (see supplemental note). The study was approved by the ethics committees of all participating institutes. Informed consent was obtained from all participants at the beginning of the study.

Whole-exome sequencing and bioinformatics analysis

Blood samples were collected from subjects, and genomic DNA was extracted with a DNA extraction kit (QIAGEN, Hilden, Germany). Library construction, whole-exome sequencing (WES), and data analysis were then performed as per methods described previously.[20,21] Briefly, genomic DNA was prepared with the Agilent SureSelect Human All Exon V6 Kit and sequenced with the Illumina HiSeq 2000. After performing the removal of adaptors, raw reads were aligned to the human genome assembly GRCh37/hg19 via the Burrows–Wheeler Aligner.[22] We then used the ANNOVAR software to conduct functional annotation with information obtained from multiple public databases and *in silico* tools, including the 1000 Genomes Project, gnomAD, Gene Ontology, SIFT, and PolyPhen-2.[23–26] Deleterious missense variants were predicted with SIFT, MutationTaster, PolyPhen-2, and combined annotation-dependent depletion (CADD) score. We determined conservation across species by performing alignment of the amino acid sequences of DNAH10 proteins whose data were obtained from the GenBank database. We further validated *DNAH10* variants identified by WES by conducting Sanger sequencing with the primers listed in Table S1.

Semen parameter analysis

Semen samples were collected through masturbation after MMAF-affected individuals observed 3–5 days of sexual abstinence, and the samples were analyzed in the source laboratories during routine biological examination, according to the World Health Organization (WHO, 2010) guidelines.[27] We used hematoxylin and eosin (H&E) staining to assess sperm morphology. Multiple flagellar malformations, including absent, short, coiled, bent, and irregular flagella, were assessed.[4] For each subject, we examined at least 200 spermatozoa to evaluate the percentages of morphologically abnormal spermatozoa.

For estimation of sperm counts and for conduction of motility analyses of the different genotypes of male mice, spermatozoa were collected from the epididymides and diluted in 1 mL human tubal fluid (HTF, MR-070-D, Millipore, Massachusetts, USA) for 15 min at 37°C. Sperm counts were determined via a hemocytometer under a light microscope, and sperm mobility was assessed via application of a computer-assisted sperm analysis (CASA) system with spermatozoa obtained from the cauda epididymides.

Scanning electron microscopy

Semen samples were prepared as per previously described methods.[7] Briefly, sperm specimens were subjected to fixation in 2.5% glutaraldehyde; thereafter, washing steps in 0.1 mol/L phosphate buffer for 30 min and post-fixation in osmic acid were conducted. Next, the specimens were subjected to washing steps again in 0.1 mol/L phosphate buffer for 30 min; thereafter, progressive dehydration with ethanol and isoamyl acetate gradient and subjection to drying conditions with a CO_2 critical-point dryer (Eiko HCP-2, Hitachi, Tokyo, Japan) were conducted. Subsequently, the specimens were mounted on aluminum stubs, sputter-coated with an ionic sprayer meter (Eiko E-1020, Hitachi, Tokyo, Japan), and analyzed via scanning electron microscopy (SEM) (Stereoscan 260, Hitachi, Tokyo, Japan) under an accelerating voltage of 20 kV.

Transmission electron microscopy

Sperm samples of participating individuals were treated as per methods described previously.[28] Briefly, the prepared spermatozoa were subjected to washing steps and fixation with 2.5% glutaraldehyde (G5882, Sigma-Aldrich, St. Louis, USA) and osmium tetroxide; thereafter, post-fixation with OsO4 and sucrose and dehydration with graded concentrations of ethanol were conducted. Subsequently, the samples were embedded in Epon 812, dodecenylsuccinic anhydride, methylnadic anhydride, and dimethylaminomethyl phenol. Ultrathin 80-nm-thick sections were stained with uranyl acetate and lead citrate and were then observed and photographed via transmission electron microscopy (TEM) (TECNAI-10, Philips; HT7700, Hitachi, Tokyo, Japan) at an accelerating voltage of 80 kV. For TEM analysis of mouse sperm, cauda epididymis samples were prepared as per methods described previously.[29]

Mouse models

Dnah10-knockout mice and $Dnah10^{M/M}$ mice were generated via the CRISPR-Cas9 genome-editing technology as per previously described methods.[30] Briefly, to generate *Dnah10*-knockout mice,

we designed single-guide RNAs (sgRNA-1: ATCTTATGCTGGGTCCAGTAAGG, sgRNA-2: TTTATAACAAATGGCTTGATTGG) against exons 2 and 5 of *Dnah10*. For generating $Dnah10^{M/M}$ mice, we designed a single-guide RNA (sgRNA-3: AGATGTGAGGGATGTGCCCAAGG) to target exon 76 of *Dnah10* with a mutation (c.13198G>A) equivalent to that observed in MMAF-affected individual T012 II-2 (c.12838G>A). We transcribed Cas9 mRNA and sgRNAs by using T7 RNA polymerase *in vitro* and then mixed and co-microinjected them into the fertilized oocytes of C57BL/6 mice. The founder mouse and its offspring were genotyped via PCR and Sanger sequencing of the tail genomic DNA with the specific primers listed in Table S2. Adult mice (aged 6 weeks or older) were used in this study. All animal procedures were conducted according to the protocols established by the Guide for the Care and Use of Laboratory Animals of the National Institutes of Health as well as the Institutional Animal Care and Use Committee of Central South University.

Reverse-transcription PCR

For conducting reverse-transcription PCR (RT-PCR), we extracted total RNA from various tissues of wild-type (WT) adult C57BL/6N mice by using the TRIzol reagent (15596026, Invitrogen, Carlsbad, USA). Approximately 1 μg RNA was reverse transcribed into cDNA via the goScript reverse-transcription system (A5000, Promega, Madison, USA) according to the manufacturer's instructions. We normalized the mRNA expression levels of *Dnah10* to those of the *Gapdh* by using the primers listed in Table S3.

Immunofluorescence analysis

For conducting immunofluorescence protein localization, we subjected the spermatozoa or selected germ cells to washing steps in phosphate-buffered saline (PBS) and subjected them to fixation onto slides with 4% paraformaldehyde for 30 min; thereafter, we permeabilized them by using 0.5% Triton X-100 for 10 min and blocked them with 10% donkey serum for 1 h at 25°C. The slides were sequentially incubated overnight at 4°C with the following primary antibodies: rabbit polyclonal anti-DNAH10 (bs-11022R, Bioss, 1:100), anti-DNAI1 (BS90420, Bioworld, 1:200), anti-DNAH2 (HPA067103, Sigma-Aldrich, 1:100), anti-DNAH8 (bs-14367R, Bioss, 1:100), anti-DNAH17 (HPA024354, Sigma-Aldrich, 1:200), anti-DNAH6 (ab122333, Abcam, 1:100), anti-SPAG6 (HPA038440, Sigma-Aldrich, 1:100), anti-AKAP4 (HPA020046, Sigma-Aldrich, 1:100), and monoclonal mouse anti-α-tubulin (T5168, Sigma-Aldrich, 1:1,000). We then subjected the slides to washing steps with PBS containing 0.1% (v/v) Tween-20 before performing a 1 h incubation at 37°C with highly cross-adsorbed secondary antibodies, namely Alexa Fluor 488 anti-mouse IgG (A21121, Life Technologies, 1:500) and Alexa Fluor 555 anti-rabbit IgG (A31572, Life Technologies, 1:500). Finally, we subjected the slides to counterstaining with 4′,6-diamidino-2-phenylindole (DAPI) to label the nuclei for 5 min at room temperature. Fluorescence signals generated as a result of the staining procedure were photographed with the Olympus IX51 fluorescence microscope (Olympus, Tokyo, Japan) and analyzed with the VideoTesT-FISH 2.0 software.

Results

Identification of bi-allelic *DNAH10* variants in men with asthenoteratozoospermia

We performed WES and bioinformatics analyses in accordance with our established protocol to investigate potential genes associated with MMAF. We identified five men from four unrelated Chinese families harboring bi-allelic *DNAH10* variants (MIM: 605884; GenBank: NM_207437.3), accounting for 0.78% (5/643) of the cohort. Individuals T012 II-2 and T089 II-1 from two unrelated consanguineous families were shown to harbor the *DNAH10* homozygous missense variants c.12838G>A (p.Gly4280Arg) and c.7601C>T (p.Thr2534Met), respectively. Individual H049 II-2, from a non-consanguineous family, harbored *DNAH10* compound heterozygous missense variants c.5663G>A (p.Arg1888Gln) and c.11887C>T (p.Arg3963Cys). Individuals NK067 II-1 and NK067 II-2, from another non-consanguineous family, harbored *DNAH10* compound heterozygous frameshift variants c.7260dup (p.Glu2421Argfs*26) and c.12235del (p.Ser4079Alafs*5) (Figure 1A and Table 1). All the mentioned *DNAH10* variants were rare or absent from public human databases, including the 1000 Genomes Project and gnomAD (v.2.1.1, 141,456 samples) (Table 1). These *DNAH10* missense variants were also predicted to be deleterious via the SIFT, MutationTaster, PolyPhen-2, and CADD tools (Table 1). Subsequent Sanger sequencing confirmed that these bi-allelic *DNAH10* variants, except for c.7601C>T (p.Thr2534Met), which could not be identified because of the lack of available DNA samples from the family members of subject T089 II-1, were inherited from heterozygous parental carriers (Figure 1B). Of note, the parents are consanguineous, suggesting the likelihood of the inheritance of this *DNAH10* missense variant under a recessive mode of inheritance.

DNAH10 (GenBank: NM_207437.3) is located on human chromosome 12 and encodes an IDA heavy chain protein. All altered amino acids were located within the conserved domain or regions of DNAH10, including its ATPase domains and dynein heavy chain (Figure S1A). Phylogenic analysis revealed that the altered residues in DNAH10 were highly conserved across species (Figure S1B). DNAH10 is abundantly expressed in the human testis according to the information presented in the Human Protein Atlas. Our RT-PCR data from various tissues of adult WT male mice also indicated that *Dnah10* was predominantly expressed in the testes and highly elevated from postnatal day 21, corresponding to the spermiogenesis stage (Figures S2A and S2B). *DNAH10* expression was also detected in ciliated cells, such as the trachea and fallopian tube (Figure S2A). Additionally, immunostaining analysis of testes samples obtained from WT mice revealed that DNAH10 was localized in the cytoplasm of elongated spermatozoa (Figure S2C). These findings further suggested that the identified bi-allelic *DNAH10* variants could be responsible for the observed infertility phenotypes.

Asthenoteratozoospermia phenotypes in men harboring bi-allelic *DNAH10* variants

Semen parameters of men harboring bi-allelic *DNAH10* variants were analyzed according to the WHO guidelines.[27] Semen analysis indicated that sperm motility

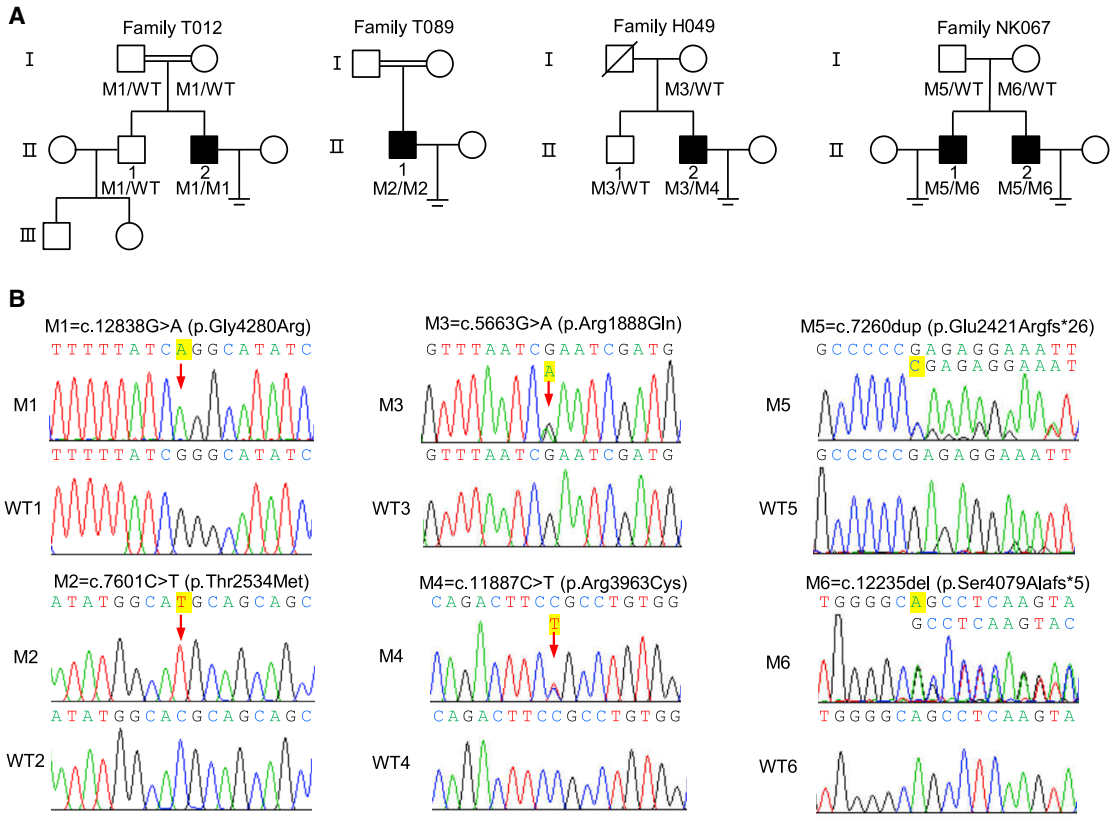

Figure 1. Identification of bi-allelic *DNAH10* variants in men with asthenoteratozoospermia
(A) Pedigrees of four families affected by *DNAH10* variants (M1–M6) identified via WES. Male individuals with asthenoteratozoospermia in these families are indicated by black-filled squares. The double lines indicate first-degree consanguinity.
(B) Sanger sequencing confirmed the presence of bi-allelic *DNAH10* variants (M1–M6) in T012 II-2, T089 II-1, H049 II-2, NK067 II-1, and NK067 II-2. The variant positions are indicated by using red arrows. WT, wild-type.

and progressive motility were severely reduced in men harboring bi-allelic *DNAH10* variants (Table S4). Sperm morphological analysis was based on H&E staining and SEM. Compared to the spermatozoa of healthy control individuals, which exhibited long smooth tails with normally condensed heads, the spermatozoa obtained from men harboring bi-allelic *DNAH10* variants exhibited frequently abnormal flagella, including absent, coiled, short, bent, and irregular caliber flagella (Figures 2A and 2B, Table S4).

Sperm samples for additional phenotypic characterization were obtained from three men harboring bi-allelic *DNAH10* variants (subjects T012 II-2, NK067 II-1, and NK067 II-2). To investigate the pathogenicity of the identified bi-allelic *DNAH10* variants, we conducted DNAH10 immunostaining of sperm cells obtained from the three MMAF-affected individuals and a control subject. DNAH10 was localized along the sperm flagella in samples obtained from the control individual but was almost absent in the sperm flagella in samples obtained from men harboring bi-allelic *DNAH10* variants (Figure 3). These results indicated that DNAH10 deficiency due to the presence of bi-allelic *DNAH10* variants might cause MMAF-related asthenoteratozoospermia.

DNAH10 variants cause MMAF with combined loss of IDAs

To investigate the sperm flagellar ultrastructure of men harboring bi-allelic *DNAH10* variants, we performed TEM analyses of samples obtained from three men harboring bi-allelic *DNAH10* variants (subjects T012 II-2, NK067 II-1, and NK067 II-2). Compared to the typical "9 + 2" axoneme microtubule structure observed in the spermatozoa obtained from control men (Figure 4), the sperm flagella of men harboring bi-allelic *DNAH10* variants mainly exhibited axoneme ultrastructural defects with the absence of IDAs (Figure 4) and a dramatic disorganization of axonemal or peri-axonemal structures (including disorganized peripheral microtubule doublets, mitochondrial sheath, outer dense fibers, and fibrous sheath, as well as absent central pair of microtubules [CP]). Quantification of cross-sections of the sperm flagella indicated higher rates of ultrastructural defects with the absence of IDAs in men harboring bi-allelic *DNAH10* variants compared to those observed in the normal control (Table S5).

To further investigate the ultrastructural defects revealed by TEM, we examined the presence and localization of several proteins belonging to different substructures of the axoneme, including DNAH2 and DNAH6 (components of

Table 1. Bi-allelic *DNAH10* variants identified in Chinese MMAF-affected men

	T012 II-2	T089 II-1	H049 II-2		NK067 II-1, II-2	
cDNA alteration	c.12838G>A	c.7601C>T	c.5663G>A	c.11887C>T	c.12235del	c.7260dup
Variant allele	p.Gly4280Arg	p.Thr2534Met	p.Arg1888Gln	p.Arg3963Cys	p.Ser4079Alafs*5	p.Glu2421Argfs*26
Variant type	homozygous	homozygous	heterozygous	heterozygous	heterozygous	heterozygous
Allele frequency in human population						
1000 Genomes Project	0	0	0	0	0	0
East Asians in gnomAD	0	0	0	0	0	0
All individuals in gnomAD	0.00005206	0.00001218	0.00000406	0.00000832	0	0
Functional prediction						
SIFT	damaging	damaging	damaging	damaging	NA	NA
PolyPhen-2	damaging	damaging	damaging	damaging	NA	NA
MutationTaster	damaging	damaging	damaging	damaging	NA	NA
CADD	27.7	28.6	6.8	8.2	NA	NA

NCBI reference sequence number of *DNAH10* is GenBank: NM_207437.3. Variants with CADD values greater than 4 are considered to be deleterious. NA, not available.

IDAs), DNAH8, DNAH17, and DNAI1 (components of ODAs), SPAG6 (component of CP), and AKAP4 (component of the fibrous sheath). We observed that DNAH2 and DNAH6 expression was remarkably reduced in the spermatozoa obtained from men harboring bi-allelic *DNAH10* variants (Figures 5A and 5B). Consistently, the AKAP4 signaling in the sperm flagella of individuals with bi-allelic *DNAH10* variants is also mislocalized along the sperm tail (Figure S3). In contrast, immunostaining results for DNAH8, DNAH17, DNAI1, and SPAG6 were comparable to those observed in controls (Figures S4, S5, S6, and S7), suggesting that ODAs and CP were not directly affected by the presence of *DNAH10* variants.

Dnah10-knockout male mice resemble asthenoteratozoospermia phenotypes

To further confirm the phenotypes caused by *DNAH10* defects in humans, we developed a *Dnah10*-knockout ($Dnah10^{-/-}$) mouse model by deleting exons 2-5 of *Dnah10* using the CRISPR-Cas9 system (Figure S8A). The founder animals were genotyped via Sanger sequencing, and the mutant mice were further confirmed via RT-PCR analysis (Figure S8B). Further, no *Dnah10* mRNA was detected in *Dnah10*-knockout testes (Figure S8B). Immunostaining results revealed that DNAH10 was absent in both the spermatozoa and testis obtained from $Dnah10^{-/-}$ male mice compared to the controls (Figures S2C and S8C). After confirming *Dnah10* deficiency in $Dnah10^{-/-}$ mice, we investigated the fertility of $Dnah10^{-/-}$ male mice. $Dnah10^{-/-}$ male mice demonstrated complete infertility (Figure 6A), as evidenced by the failure in offspring production after mating. We also compared testis weights and sizes between $Dnah10^{+/-}$ and $Dnah10^{-/-}$ male mice, but no significant differences were observed (Figure 6B).

Subsequently, we investigated the semen characteristics, as well as sperm morphology and ultrastructure in $Dnah10^{-/-}$ male mice. The epididymal spermatozoa of $Dnah10^{-/-}$ male mice showed significant reduction in count and demonstrated 100% immotility in contrast to those of $Dnah10^{+/-}$ male mice (Figures 6C and 6D). Compared to the spermatozoa of $Dnah10^{+/-}$ male mice, which presented long, smooth tails with normally condensed heads, the flagella of all spermatozoa obtained from $Dnah10^{-/-}$ male mice exhibited multiple abnormalities, including absent, coiled, short, and irregular flagella, which recapitulated the clinical phenotypes of MMAF-affected men with bi-allelic *DNAH10* variants (Figure 6E and Table S6). Furthermore, TEM analysis indicated a disorganized mitochondrial sheath, outer dense fibers, and microtubules in the flagella of sperm obtained from $Dnah10^{-/-}$ male mice (Figure 6F).

To further investigate the role of DNAH10 in spermatogenesis, we performed H&E staining of the testis samples of $Dnah10^{+/-}$ and $Dnah10^{-/-}$ male mice. No elongated tails were observed in stage VII–VIII seminiferous tubules of $Dnah10^{-/-}$ male mice testes. Instead, normal round spermatids were observed (Figure S9), indicating the involvement of DNAH10 in sperm flagellar formation. Collectively, these data suggested that DNAH10 deficiency could result in the development of MMAF and male infertility in both humans and mice.

Asthenoteratozoospermia phenotypes in $Dnah10^{M/M}$-knockin male mice

To further explore whether the *DNAH10* variants were indeed the pathogenic cause of MMAF in affected men, we developed a knockin mouse model ($Dnah10^{M/M}$) with mice that harbored a homozygous *Dnah10* variant (c.13198G>A) (Figure S10A), corresponding to the *DNAH10* variant (c.12838G>A) in MMAF-affected individual T012 II-2, via application of the CRISPR-Cas9 technology. We performed PCR and Sanger sequencing to confirm

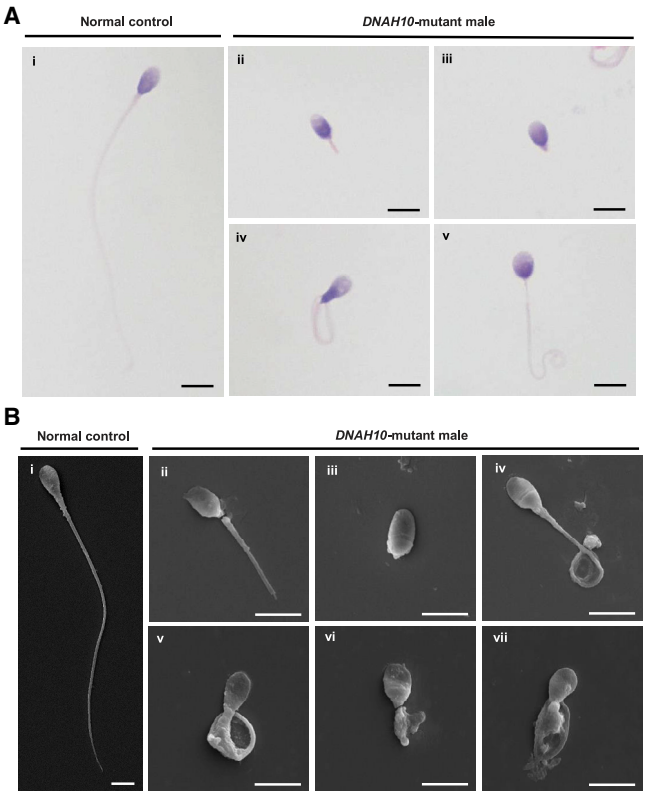

Figure 2. Sperm morphology analyses for men harboring bi-allelic *DNAH10* variants

(A) H&E staining for the spermatozoa obtained from a fertile control individual (NC) and men harboring bi-allelic *DNAH10* variants. Compared to the spermatozoa of NC, which presented long, smooth tails (i), most spermatozoa obtained from men harboring *DNAH10* variants displayed typical MMAF phenotypes, such as short (ii), absent (iii), coiled (iv), and irregular flagella (v). The data of H049 II-2 are shown as an example. Scale bars, 5 μm. (B) SEM analysis of the spermatozoa obtained from a fertile control individual (NC) and men harboring bi-allelic *DNAH10* variants. (i) Normal morphology of the spermatozoon from a healthy control male. (ii–vii) Most spermatozoa obtained from men harboring bi-allelic *DNAH10* variants displayed typical MMAF phenotypes, including short (ii), absent (iii), bent (iv), coiled (v), and irregular flagella (vi and vii). The data of H049 II-2 are shown as an example. Scale bars, 5 μm.

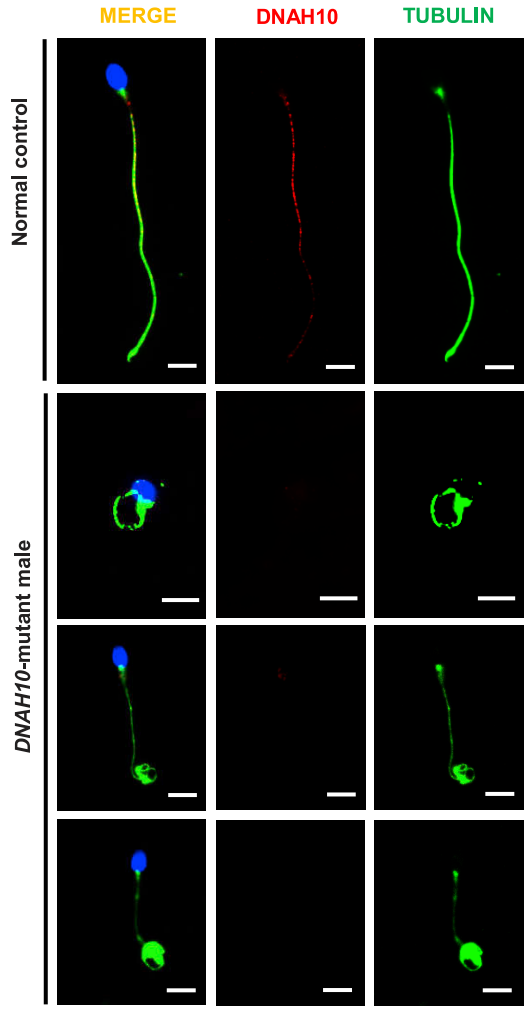

Figure 3. Expression analysis of DNAH10 in the spermatozoa obtained from a male control individual and men harboring bi-allelic *DNAH10* variants

Representative images of spermatozoa obtained from a fertile control individual (NC) and men harboring bi-allelic *DNAH10* variants (T012 II-2, NK067 II-1, and NK067 II-2) stained with the anti-DNAH10 antibody, anti-α-tubulin antibody, and DAPI. Staining results revealed that DNAH10 was localized along the sperm flagella in the sperm obtained from the NC but was almost absent in the sperm flagella in the sperm obtained from men harboring bi-allelic *DNAH10* variants. Representative data are provided to illustrate the typical staining observed in *DNAH10*-associated cases. Scale bars, 5 μm.

the mutated allele in *Dnah10*$^{M/M}$ mice (Figure S10B). Immunostaining results revealed that DNAH10 was reduced in both the spermatozoa and testis obtained from *Dnah10*$^{M/M}$ male mice compared to those obtained from the controls (Figures S10C and S11). Subsequently, we investigated the fertility of *Dnah10*$^{M/M}$ male mice. As expected, *Dnah10*$^{M/M}$ male mice exhibited complete infertility after conduction of mating with *Dnah10*$^{+/M}$ female mice (Figure 7A), whereas *Dnah10*$^{M/M}$ female mice showed complete fertility as evidenced by the production of litters of normal size compared to those of *Dnah10*$^{+/+}$ female mice (data not shown). No evident anomalies or differences were observed in size and weight between *Dnah10*$^{M/M}$ and *Dnah10*$^{+/M}$ male mouse testes (Figure 7B).

We further investigated the semen characteristics and sperm morphology in *Dnah10*$^{M/M}$ male mice. Compared to that observed in *Dnah10*$^{+/M}$ mice, sperm concentration was significantly reduced and was associated with a complete motility deficiency in *Dnah10*$^{M/M}$ male mice (Figures 7C and 7D). Epididymal sperm obtained from *Dnah10*$^{M/M}$ male mice displayed a phenotype identical to typical human MMAF; all spermatozoa exhibited absent, coiled, short, and irregular flagella (Figure 7E and Table S6). Furthermore, TEM analysis showed a disorganized mitochondrial sheath, outer dense fibers, and absence of microtubules in the midpiece of flagella in sperm obtained from *Dnah10*$^{M/M}$ male mice (Figure 7F). Importantly, H&E staining analysis of stage VII–VIII seminiferous tubules in samples obtained from *Dnah10*$^{+/M}$ and *Dnah10*$^{M/M}$ male mice

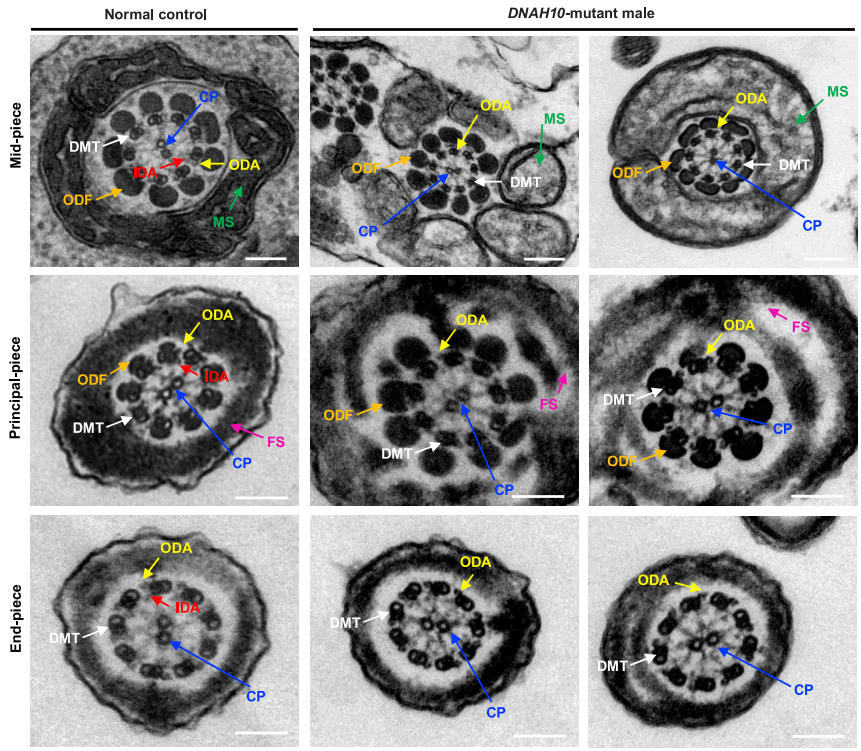

Figure 4. Sperm ultrastructure analyses for men harboring bi-allelic *DNAH10* variants

TEM analysis of spermatozoa obtained from a fertile control individual (NC) and men harboring bi-allelic *DNAH10* variants. Cross-sections of the midpiece and principal piece of the sperm flagella in the sperm obtained from NC displayed typical "9 + 2" microtubule structure and peri-axoneme structure. The axoneme microtubule structure, including nine pairs of peripheral doublet microtubules (DMT; indicated with white arrows) and the central pair of microtubules (CP; indicated with blue arrows), is visible. The outer dynein arms (ODA; indicated with yellow arrows) and inner dynein arms (IDA; indicated with red arrows) are also visible. The peri-axoneme structure includes a helical mitochondrial sheath (MS; indicated with green arrows), nine outer dense fibers (ODFs; indicated with orange arrows), and the fiber sheath (FS; indicated with pink arrows). Cross-sections of the midpiece, principal piece, and endpiece of the spermatozoa obtained from men harboring bi-allelic *DNAH10* variants revealed typical axonemal anomalies with the absence of inner dynein arms, while other axoneme microtubule structures seemed to be unaffected. The data of NK067 II-1 and NK067 II-2 are shown as an example. Scale bars, 200 nm.

revealed the absence of elongated tails in the testes of *Dnah10*$^{-/-}$ male mice. Instead, normal round spermatids were observed (Figure S12). Hence, consistent with the findings in MMAF-affected individuals, the sperm phenotypes of *Dnah10*$^{M/M}$ male mice further indicated that the *DNAH10* variant (c.12838G>A) was indeed pathogenic for male fertility due to asthenoteratozoospermia.

Discussion

Our WES analyses of 643 Chinese men with MMAF identified five individuals carrying bi-allelic variants of *DNAH10*, which encodes an axonemal IDA heavy chain component that is preferentially expressed in the testes. These *DNAH10* variants were rare or absent from human public datasets archived in the 1000 Genomes Project and gnomAD (Figure 1 and Table 1). The evidence obtained from functional experiments combined with analyses using *Dnah10*-knockout/-knockin male mice consistently indicated that *DNAH10* was an MMAF-associated gene.

Dyneins are the main components of multi-subunit motor protein complexes that harness the energy of ATP hydrolysis for ciliary and flagellar motility.[15] Dyneins are arranged in complex arrays of single-headed, heterodimeric, and heterotrimeric ODA and IDA complexes.[31] The mammalian IDAs, which are responsible for ciliary and flagellar beating, are complex structures regularly attached to peripheral A-microtubules.[15,31] Previous studies reported the existence of two types of human IDAs, including the single-headed IDA subspecies (i.e., DNALI1, DNAH1, DNAH6, and DNAH12) and heterodimeric IDA-I1 complex (i.e., DNAH2 and DNAH10). Deficiency of both types of human IDA-associated proteins reportedly result in asthenoteratozoospermia with or without the manifestation of other PCD symptoms. For example, disruption of *DNAH1* is responsible for the development of both asthenoteratozoospermia and PCD,[4,32] while mutations in *DNAH2* and *DNAH6* are associated with asthenoteratozoospermia without the occurrence of other PCD symptoms.[18,33] These previous observations indicate that IDA-associated proteins play important roles in ciliary and flagellar morphology and motility.

Our phenotypic analysis revealed that men harboring bi-allelic *DNAH10* variants displayed typical MMAF phenotypes, including reduced sperm motility and multiple morphological abnormalities of the sperm flagella, without the occurrence of other PCD symptoms. The sperm concentrations vary a lot among males with *DNAH10* mutation. Interestingly, similar differences in sperm phenotype were also reported for other MMAF-related genes, such as *ARMC2*, *CFAP47*, *CFAP251*, *DNAH8*, and *TTC29*.[8,34–37] We did not observe a significant difference in sperm concentration between the males with *DNAH10* mutation and the individuals with mutations in other MMAF-related genes, such as *ARMC2*, *CFAP47*, *CFAP251*, *DNAH8*, and *TTC29*. The cause of variable sperm concentration may be partially due to

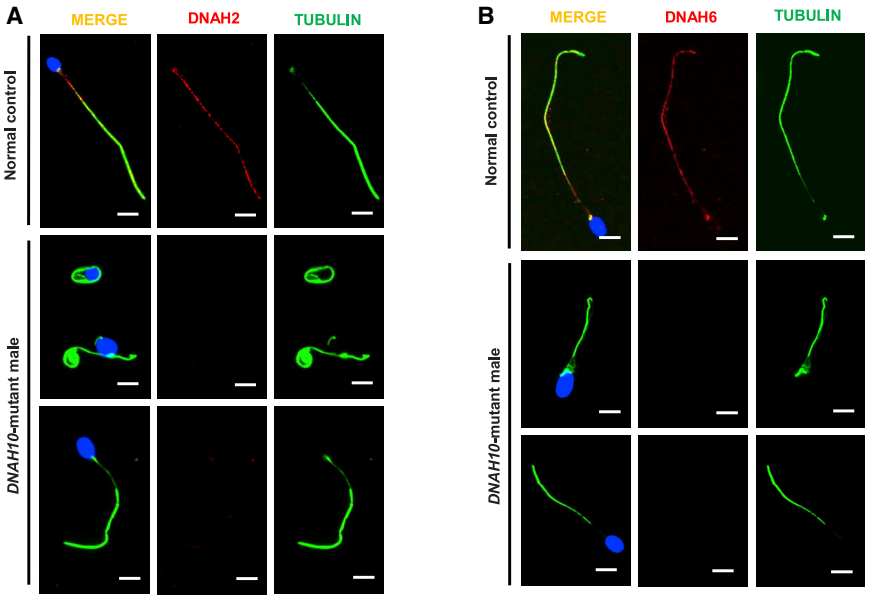

Figure 5. DNAH2 and DNAH6 immunostaining is altered in spermatozoa obtained from men harboring bi-allelic *DNAH10* variants

(A and B) The spermatozoa obtained from a fertile control individual (NC) and men harboring bi-allelic *DNAH10* variants were stained with anti-DNAH2 (indicated as red in [A]), anti-DNAH6 (indicated as red in [B]), anti-a-tubulin (indicated as green) antibodies, and DAPI (indicated as blue). DNAH2 and DNAH6 normally localized along the sperm flagella in the control sperm. However, expression of both DNAH2 and DNAH6 was almost absent in the sperm obtained from men harboring bi-allelic *DNAH10* variants. Scale bars, 10 μm.

individual heterogeneity, phenotypic heterogeneity of MMAF-related genes, and/or differences in environmental exposure and lifestyle among males with *DNAH10* mutation.

A previous study conducted with an antibody recognizing the N terminus of DNAH10 (amino acids 781–900) has reported that DNAH10 is expressed in both human respiratory cilia and sperm flagella.[38] However, we only detected DNAH10 in the sperm flagella (Figure 3), and not in respiratory cilia (Figure S13), by using an antibody recognizing the DNAH10 C terminus (amino acids 3561–3700). This observation supports the importance of DNAH10 in normal sperm tail assembly. In our study, the identified DNAH10 variants showed alterations at the C terminus, and men harboring these variants presented with isolated male infertility. Considering the different expression patterns among distinct *DNAH10* transcripts (Figure S2A), we speculated that variants at the N terminus of DNAH10 might be responsible for the development of both male infertility and PCD-like symptoms. Consistently, our group and others observed that mutations at distinct positions of *SPEF2* in different individuals as well as mutant mice resulted in variable phenotypes, including male infertility and/or PCD-like symptoms.[28,39–42] Therefore, further investigation in larger MMAF and PCD cohorts should be conducted to validate this speculation.

In this study, TEM revealed marked axoneme ultrastructural defects in men harboring bi-allelic *DNAH10* variants, and approximately 80% of the axoneme cross-sections exhibited axonemal malformations. The main defect types comprised the absence of IDAs. Intriguingly, the loss of IDAs was associated with a global and severe disorganization of the axonemal structure, including missing CP and microtubule doublets. In agreement with this finding, other IDA-associated proteins exhibited similar ultrastructural defects in the sperm flagellum phenotype. For example, spermatozoa obtained from men with *DNAH1* or *DNAH2* mutations exhibited severely disarranged axonemal structures with loss of IDAs.[4,18] The pathophysiological mechanisms underlying the occurrence of this sperm-specific phenotype due to mutations in IDA-associated proteins are probably attributable to axonemal assembly and/or stability defects.

Moreover, we established *Dnah10*-mutated mice in this study to further explore the effect of DNAH10 deficiency on sperm flagellar formation. Consistent with the clinical presentation of men harboring bi-allelic *DNAH10* variants, *Dnah10*-mutated male mice were sterile and displayed a typical MMAF phenotype, including completely immotile sperm and abnormal flagella. H&E staining revealed abnormal spermiogenesis in the testes and reduced sperm counts in the cauda epididymis of *Dnah10*-mutated male mice. Notably, the sperm phenotype of *Dnah10*-mutated male mice appears more severe than the phenotype of men harboring bi-allelic *DNAH10* variants. Interestingly, we noticed that the differences in sperm phenotypes between humans and mice were also observed in other MMAF-related genes, such as *TTC29*, *CFAP47*, and *DNAH8*.[36,37,43] This might be due to evolutionarily divergent protein interaction networks between humans and mice as predicted by the *in silico* tool STRING (Figure S14) or distinct compensatory mechanisms between species or differences in environmental exposure.

We also developed *Dnah10*-knockin mice with a mutation equivalent to that observed in one MMAF-affected individual, T012 II-2 (c.12838G>A), to further explore the pathogenicity of the *DNAH10* variant. Consistent with the clinical presentation of men harboring bi-allelic *DNAH10* variants and *Dnah10*-knockout male mice, *Dnah10*-knockin male mice were sterile because of the presence of an MMAF phenotype. Therefore, mutant mouse models with the corresponding *DNAH10* missense mutation provided further evidence supporting the role of *DNAH10* as an MMAF-associated gene.

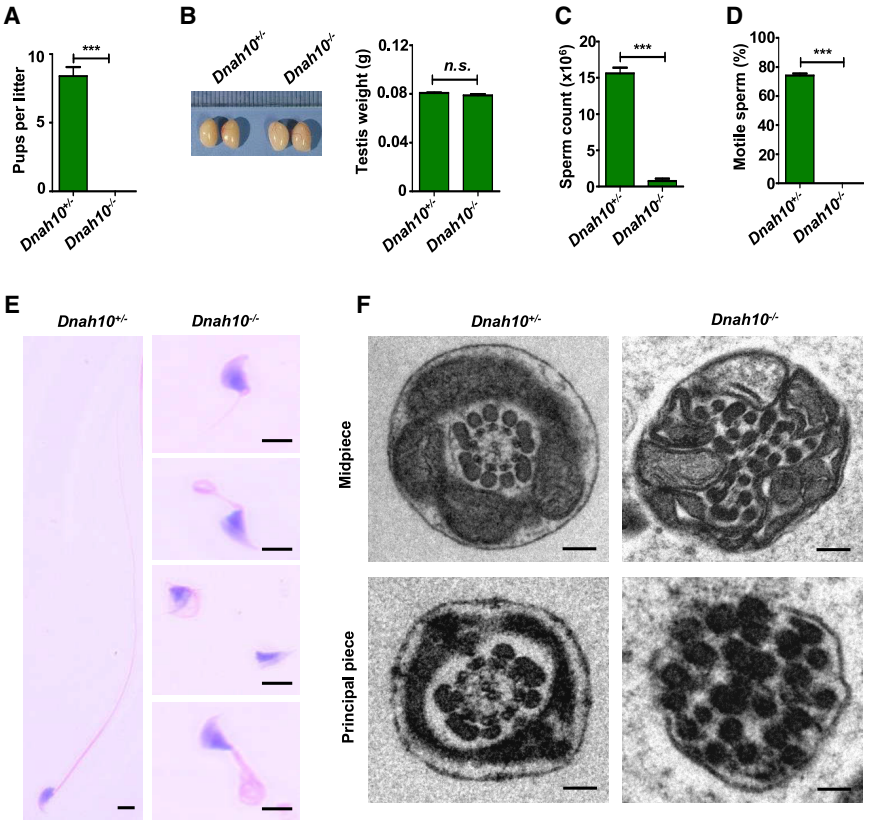

Figure 6. *Dnah10* deficiency results in typical MMAF phenotypes and infertility in male mice

(A) Fertility test of male mice at 2–5 months of age after mating with $Dnah10^{+/-}$ females (***$p < 0.001$).

(B) The size (left) and weight (right) of testes were comparable between $Dnah10^{-/-}$ and $Dnah10^{+/-}$ male mice at 2 months of age. n.s., not significant.

(C) The sperm concentration of $Dnah10^{-/-}$ male mice was significantly lower than that of $Dnah10^{+/-}$ male mice (***$p < 0.001$).

(D) Percentages of motile sperms in $Dnah10^{-/-}$ male mice and $Dnah10^{+/-}$ male mice at 2 months of age (***$p < 0.001$).

(E) H&E staining of the spermatozoa obtained from mouse cauda epididymis. When compared with the normal morphology of spermatozoa obtained from $Dnah10^{+/-}$ male mice, $Dnah10^{-/-}$ male mouse spermatozoa exhibited aberrant flagellar morphologies, which were consistent with the clinical phenotypes observed in men harboring bi-allelic *DNAH10* variants.

(F) Cross-sectional ultrastructure of cauda epididymal spermatozoa obtained from $Dnah10^{-/-}$ male mice and $Dnah10^{+/-}$ male mice at 2 months of age via TEM. Compared with the normal ultrastructure in $Dnah10^{+/-}$ male mice, cross-sections of the midpiece and principal piece of the sperm flagella in $Dnah10^{-/-}$ male mice revealed disorganization of the axoneme, mitochondrial sheaths, and outer dense fibers. Scale bars, 100 nm.

Intra-machette protein transport (IMT) and intra-flagella protein transport (IFT) are two highly evolutionarily conserved bidirectional transport platforms and are essential for sperm head shaping and protein transport into the tail.[44] IMT and IFT are both based on microtubular tracks and use motors for the trafficking of cargo-related transport complexes, such as structural components of the axoneme, fiber sheath, and peripheral dense fiber.[44–46] In this study, the sperm cytology in Figures 6E and 7E reveals club-shaped head morphology and deformed flagellum, suggesting a defect in IFT and IMT processes. Interestingly, STRING analysis indicates that DNAH10 may be highly connected with multiple cytoplasmic dynein 1 components (such as DYNLL1, DYNC1LI2, and DYNC1LI2) as well as structural components of the axoneme (such as DNAH12, DNAI1, and CFAP46) (Figure S14A), and these cytoplasmic dynein components can be used as motors in the retrograde IFT and IMT processes.[47–50] Therefore, we speculate that the mechanism of DNAH10 deficiency leading to malformed sperm may be related to IFT and IMT processes, but it is not clear whether DNAH10 directly participates in sperm head shaping and flagellar assembly through IFT or IMT processes or affects sperm head shaping and flagellar assembly as a cargo component of IFT or IMT. An exploration of this role would be a worthy subject for a follow-up study.

From a clinical perspective, intracytoplasmic sperm injection (ICSI) exists as the only approach for conception in couples wherein the male partner is diagnosed with infertility attributable to the presence of an MMAF phenotype. Previous studies revealed the different outcomes of ICSI for a series of individuals harboring MMAF-related genes. For example, MMAF-affected individuals with bi-allelic variants in *DNAH1*, *DNAH8*, or *TTC29* have good clinical outcomes following ICSI.[36,43,51] In contrast, ICSI reportedly shows failure in MMAF-affected men harboring *CEP135* (MIM: 611423), *DNAH17*, or *CFAP65* variants.[19,21,52] Herein, we observed that among the five subjects harboring mutations in *DNAH10*, three individuals received assisted reproductive therapy by ICSI and two out of three men achieved good clinical outcomes (Table S7). We re-analyzed the clinical information of couples (H049 II-2) who experienced poor ICSI outcome. We found that the wife of individual H049 II-2 retrieved six oocytes with poor quality, leading to only three poor-quality embryos. Therefore, the factors for the failed embryo transfer cycle might together attribute to the poor-quality oocytes and the sperm quality of the individual (H049 II-2). Considering the small sample size, further investigation with the sperm from *Dnah10*-knockout/-knockin male mice should be performed to assess whether ICSI could be recommended for *DNAH10*-associated asthenoteratozoospermia.

In conclusion, we identified five men harboring bi-allelic variants of *DNAH10* in a cohort of 643 MMAF-affected Chinese men. Genetic evidence from *DNAH10*-associated men and *Dnah10*-knockout and -knockin male mice strongly

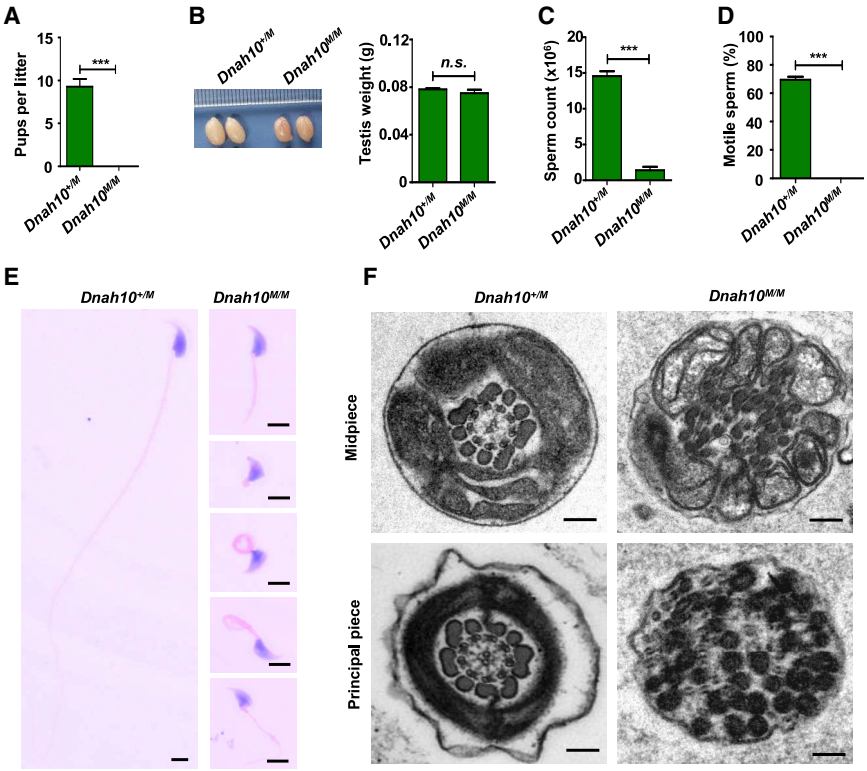

Figure 7. *Dnah10*$^{M/M}$ male mice exhibit typical MMAF phenotypes and infertility

(A) Fertility test of male mice at 2–5 months of age after mating with *Dnah10*$^{+/M}$ females (***p < 0.001).

(B) The size (left) and weight (right) of testes were comparable between *Dnah10*$^{M/M}$ and *Dnah10*$^{+/M}$ male mice at 2 months of age. n.s., not significant.

(C) The sperm concentration of *Dnah10*$^{M/M}$ male mice was significantly lower than that of *Dnah10*$^{+/M}$ male mice (***p < 0.001).

(D) Percentages of motile sperms (e) in *Dnah10*$^{M/M}$ male mice and *Dnah10*$^{+/M}$ male mice at 2 months of age (***p < 0.001).

(E) H&E staining of the spermatozoa obtained from mouse cauda epididymis. When compared with the normal morphology of spermatozoa obtained from *Dnah10*$^{+/M}$ male mice, *Dnah10*$^{M/M}$ male mouse spermatozoa exhibited aberrant flagellar morphologies, which were consistent with the clinical phenotypes in men harboring bi-allelic *DNAH10* variants.

(F) Cross-sectional ultrastructure of cauda epididymal spermatozoa obtained from *Dnah10*$^{M/M}$ male mice and *Dnah10*$^{+/M}$ male mice at 2 months of age via TEM. Compared with the normal ultrastructure in *Dnah10*$^{+/M}$ male mice, cross-sections of the midpiece and principal piece of the sperm flagella in *Dnah10*$^{M/M}$ male mice revealed disorganization of the axoneme, mitochondrial sheaths, and outer dense fibers. Scale bars, 100 nm.

suggests that bi-allelic *DNAH10* variants can induce asthenoteratozoospermia characterized by reduced sperm motility and multiple sperm malformations. Further studies using *Dnah10*-knockout/-knockin mouse models may help in the elucidation of the molecular mechanisms underlying the function of DNAH10 in sperm flagellogenesis.

Data and code availability

The WES datasets supporting the current study have not been deposited in a public repository because of privacy and ethical restrictions but are available from the corresponding authors on request.

Supplemental information

Supplemental information can be found online at https://doi.org/10.1016/j.ajhg.2021.06.010.

Acknowledgments

We would like to thank the families for participating and supporting this study. We also thank the Center of Cryo-electron Microscopy at Central South University and Zhejiang University for technical support. This work was supported by the National Key Research and Developmental Program of China (2018YFC1004900, 2018YFC1003603, and SQ2019YFC100008), The National Natural Science Foundation of China (81771645, 81971447, 81601340, 31625015, 31521003, 81971441, and 81901541), China Postdoctoral Science Foundation (2019M662786), the research grant of CITIC-Xiangya (YNXM-201915, YNXM-201913, YNXM-201912, and YNXM-201916), the Hunan Provincial Natural Science Foundation of China (2020JJ5993), the key grant of prevention and treatment of birth defect from Hunan province (2019SK1012), the Department of Science and Technology of Anhui Province (2017070802D150), and Shanghai Municipal Science and Technology Major Project (2017SHZDZX01).

Declaration of interests

The authors declare no competing interests.

Received: March 8, 2021
Accepted: June 9, 2021
Published: July 7, 2021

Web resources

1000 Genomes Project, https://www.internationalgenome.org/
CADD, https://cadd.gs.washington.edu/snv
Database of Genomic Variations, http://dgv.tcag.ca/dgv/app/home
gnomAD, https://gnomad.broadinstitute.org
HUGO Gene Nomenclature Committee, https://www.genenames.org/
National Center for Biotechnology Information (NCBI), https://www.ncbi.nlm.nih.gov/
OMIM, https://omim.org/
Picard, https://github.com/broadinstitute/picard
PolyPhen-2, http://genetics.bwh.harvard.edu/pph2/
SIFT, https://sift.bii.a-star.edu.sg

UCSC Genome Browser, http://genome.ucsc.edu
UniProt, https://www.uniprot.org

References

1. Tournaye, H., Krausz, C., and Oates, R.D. (2017). Novel concepts in the aetiology of male reproductive impairment. Lancet Diabetes Endocrinol. *5*, 544–553.
2. Agarwal, A., Baskaran, S., Parekh, N., Cho, C.L., Henkel, R., Vij, S., Arafa, M., Panner Selvam, M.K., and Shah, R. (2021). Male infertility. Lancet *397*, 319–333.
3. Shahrokhi, S.Z., Salehi, P., Alyasin, A., Taghiyar, S., and Deemeh, M.R. (2020). Asthenozoospermia: Cellular and molecular contributing factors and treatment strategies. Andrologia *52*, e13463.
4. Ben Khelifa, M., Coutton, C., Zouari, R., Karaouzène, T., Rendu, J., Bidart, M., Yassine, S., Pierre, V., Delaroche, J., Hennebicq, S., et al. (2014). Mutations in DNAH1, which encodes an inner arm heavy chain dynein, lead to male infertility from multiple morphological abnormalities of the sperm flagella. Am. J. Hum. Genet. *94*, 95–104.
5. Wang, Z., Pan, Y., He, L., Song, X., Chen, H., Pan, C., Qu, L., Zhu, H., and Lan, X. (2020). Multiple morphological abnormalities of the sperm flagella (MMAF)-associated genes: The relationships between genetic variation and litter size in goats. Gene *753*, 144778.
6. Touré, A., Martinez, G., Kherraf, Z.E., Cazin, C., Beurois, J., Arnoult, C., Ray, P.F., and Coutton, C. (2021). The genetic architecture of morphological abnormalities of the sperm tail. Hum. Genet. *140*, 21–42.
7. Tang, S., Wang, X., Li, W., Yang, X., Li, Z., Liu, W., Li, C., Zhu, Z., Wang, L., Wang, J., et al. (2017). Biallelic Mutations in CFAP43 and CFAP44 Cause Male Infertility with Multiple Morphological Abnormalities of the Sperm Flagella. Am. J. Hum. Genet. *100*, 854–864.
8. Liu, C., Miyata, H., Gao, Y., Sha, Y., Tang, S., Xu, Z., Whitfield, M., Patrat, C., Wu, H., Dulioust, E., et al. (2020). Bi-allelic DNAH8 Variants Lead to Multiple Morphological Abnormalities of the Sperm Flagella and Primary Male Infertility. Am. J. Hum. Genet. *107*, 330–341.
9. He, X., Liu, C., Yang, X., Lv, M., Ni, X., Li, Q., Cheng, H., Liu, W., Tian, S., Wu, H., et al. (2020). Bi-allelic Loss-of-function Variants in CFAP58 Cause Flagellar Axoneme and Mitochondrial Sheath Defects and Asthenoteratozoospermia in Humans and Mice. Am. J. Hum. Genet. *107*, 514–526.
10. Sironen, A., Shoemark, A., Patel, M., Loebinger, M.R., and Mitchison, H.M. (2020). Sperm defects in primary ciliary dyskinesia and related causes of male infertility. Cell. Mol. Life Sci. *77*, 2029–2048.
11. Linck, R.W., Chemes, H., and Albertini, D.F. (2016). The axoneme: the propulsive engine of spermatozoa and cilia and associated ciliopathies leading to infertility. J. Assist. Reprod. Genet. *33*, 141–156.
12. Inaba, K. (2011). Sperm flagella: comparative and phylogenetic perspectives of protein components. Mol. Hum. Reprod. *17*, 524–538.
13. Ishikawa, T. (2017). Axoneme Structure from Motile Cilia. Cold Spring Harb. Perspect. Biol. *9*, a028076.
14. Kikkawa, M. (2013). Big steps toward understanding dynein. J. Cell Biol. *202*, 15–23.
15. Roberts, A.J., Kon, T., Knight, P.J., Sutoh, K., and Burgess, S.A. (2013). Functions and mechanics of dynein motor proteins. Nat. Rev. Mol. Cell Biol. *14*, 713–726.
16. Summers, K.E., and Gibbons, I.R. (1971). Adenosine triphosphate-induced sliding of tubules in trypsin-treated flagella of sea-urchin sperm. Proc. Natl. Acad. Sci. USA *68*, 3092–3096.
17. Pazour, G.J., Agrin, N., Walker, B.L., and Witman, G.B. (2006). Identification of predicted human outer dynein arm genes: candidates for primary ciliary dyskinesia genes. J. Med. Genet. *43*, 62–73.
18. Li, Y., Sha, Y., Wang, X., Ding, L., Liu, W., Ji, Z., Mei, L., Huang, X., Lin, S., Kong, S., et al. (2019). DNAH2 is a novel candidate gene associated with multiple morphological abnormalities of the sperm flagella. Clin. Genet. *95*, 590–600.
19. Whitfield, M., Thomas, L., Bequignon, E., Schmitt, A., Stouvenel, L., Montantin, G., Tissier, S., Duquesnoy, P., Copin, B., Chantot, S., et al. (2019). Mutations in DNAH17, Encoding a Sperm-Specific Axonemal Outer Dynein Arm Heavy Chain, Cause Isolated Male Infertility Due to Asthenozoospermia. Am. J. Hum. Genet. *105*, 198–212.
20. Shen, Y., Zhang, F., Li, F., Jiang, X., Yang, Y., Li, X., Li, W., Wang, X., Cheng, J., Liu, M., et al. (2019). Loss-of-function mutations in QRICH2 cause male infertility with multiple morphological abnormalities of the sperm flagella. Nat. Commun. *10*, 433.
21. Wang, W., Tu, C., Nie, H., Meng, L., Li, Y., Yuan, S., Zhang, Q., Du, J., Wang, J., Gong, F., et al. (2019). Biallelic mutations in *CFAP65* lead to severe asthenoteratospermia due to acrosome hypoplasia and flagellum malformations. J. Med. Genet. *56*, 750–757.
22. Li, H., and Durbin, R. (2009). Fast and accurate short read alignment with Burrows-Wheeler transform. Bioinformatics *25*, 1754–1760.
23. Wang, K., Li, M., and Hakonarson, H. (2010). ANNOVAR: functional annotation of genetic variants from high-throughput sequencing data. Nucleic Acids Res. *38*, e164.
24. Kumar, P., Henikoff, S., and Ng, P.C. (2009). Predicting the effects of coding non-synonymous variants on protein function using the SIFT algorithm. Nat. Protoc. *4*, 1073–1081.
25. Adzhubei, I.A., Schmidt, S., Peshkin, L., Ramensky, V.E., Gerasimova, A., Bork, P., Kondrashov, A.S., and Sunyaev, S.R. (2010). A method and server for predicting damaging missense mutations. Nat. Methods *7*, 248–249.
26. Ashburner, M., Ball, C.A., Blake, J.A., Botstein, D., Butler, H., Cherry, J.M., Davis, A.P., Dolinski, K., Dwight, S.S., Eppig, J.T., et al.; The Gene Ontology Consortium (2000). Gene ontology: tool for the unification of biology. Nat. Genet. *25*, 25–29.
27. Cooper, T.G., Noonan, E., von Eckardstein, S., Auger, J., Baker, H.W., Behre, H.M., Haugen, T.B., Kruger, T., Wang, C., Mbizvo, M.T., and Vogelsong, K.M. (2010). World Health Organization reference values for human semen characteristics. Hum. Reprod. Update *16*, 231–245.
28. Tu, C., Nie, H., Meng, L., Wang, W., Li, H., Yuan, S., Cheng, D., He, W., Liu, G., Du, J., et al. (2020). Novel mutations in SPEF2 causing different defects between flagella and cilia bridge: the phenotypic link between MMAF and PCD. Hum. Genet. *139*, 257–271.
29. Liu, W., He, X., Yang, S., Zouari, R., Wang, J., Wu, H., Kherraf, Z.E., Liu, C., Coutton, C., Zhao, R., et al. (2019). Bi-allelic Mutations in TTC21A Induce Asthenoteratospermia in Humans and Mice. Am. J. Hum. Genet. *104*, 738–748.
30. Wang, H., Yang, H., Shivalila, C.S., Dawlaty, M.M., Cheng, A.W., Zhang, F., and Jaenisch, R. (2013). One-step generation of mice carrying mutations in multiple genes by

CRISPR/Cas-mediated genome engineering. Cell *153*, 910–918.
31. Kollmar, M. (2016). Fine-Tuning Motile Cilia and Flagella: Evolution of the Dynein Motor Proteins from Plants to Humans at High Resolution. Mol. Biol. Evol. *33*, 3249–3267.
32. Imtiaz, F., Allam, R., Ramzan, K., and Al-Sayed, M. (2015). Variation in DNAH1 may contribute to primary ciliary dyskinesia. BMC Med. Genet. *16*, 14.
33. Tu, C., Nie, H., Meng, L., Yuan, S., He, W., Luo, A., Li, H., Li, W., Du, J., Lu, G., et al. (2019). Identification of DNAH6 mutations in infertile men with multiple morphological abnormalities of the sperm flagella. Sci. Rep. *9*, 15864.
34. Coutton, C., Martinez, G., Kherraf, Z.E., Amiri-Yekta, A., Boguenet, M., Saut, A., He, X., Zhang, F., Cristou-Kent, M., Escoffier, J., et al. (2019). Bi-allelic Mutations in ARMC2 Lead to Severe Astheno-Teratozoospermia Due to Sperm Flagellum Malformations in Humans and Mice. Am. J. Hum. Genet. *104*, 331–340.
35. Li, W., He, X., Yang, S., Liu, C., Wu, H., Liu, W., Lv, M., Tang, D., Tan, J., Tang, S., et al. (2019). Biallelic mutations of CFAP251 cause sperm flagellar defects and human male infertility. J. Hum. Genet. *64*, 49–54.
36. Liu, C., He, X., Liu, W., Yang, S., Wang, L., Li, W., Wu, H., Tang, S., Ni, X., Wang, J., et al. (2019). Bi-allelic Mutations in TTC29 Cause Male Subfertility with Asthenoteratospermia in Humans and Mice. Am. J. Hum. Genet. *105*, 1168–1181.
37. Liu, C., Tu, C., Wang, L., Wu, H., Houston, B.J., Mastrorosa, F.K., Zhang, W., Shen, Y., Wang, J., Tian, S., et al. (2021). Deleterious variants in X-linked CFAP47 induce asthenoteratozoospermia and primary male infertility. Am. J. Hum. Genet. *108*, 309–323.
38. Thomas, L., Bouhouche, K., Whitfield, M., Thouvenin, G., Coste, A., Louis, B., Szymanski, C., Bequignon, E., Papon, J.F., Castelli, M., et al. (2020). TTC12 Loss-of-Function Mutations Cause Primary Ciliary Dyskinesia and Unveil Distinct Dynein Assembly Mechanisms in Motile Cilia Versus Flagella. Am. J. Hum. Genet. *106*, 153–169.
39. Sironen, A., Kotaja, N., Mulhern, H., Wyatt, T.A., Sisson, J.H., Pavlik, J.A., Miiluniemi, M., Fleming, M.D., and Lee, L. (2011). Loss of SPEF2 function in mice results in spermatogenesis defects and primary ciliary dyskinesia. Biol. Reprod. *85*, 690–701.
40. Sironen, A., Thomsen, B., Andersson, M., Ahola, V., and Vilkki, J. (2006). An intronic insertion in KPL2 results in aberrant splicing and causes the immotile short-tail sperm defect in the pig. Proc. Natl. Acad. Sci. USA *103*, 5006–5011.
41. Guo, F., Yang, B., Ju, Z.H., Wang, X.G., Qi, C., Zhang, Y., Wang, C.F., Liu, H.D., Feng, M.Y., Chen, Y., et al. (2013). Alternative splicing, promoter methylation, and functional SNPs of sperm flagella 2 gene in testis and mature spermatozoa of Holstein bulls. Reproduction *147*, 241–252.
42. Liu, C., Lv, M., He, X., Zhu, Y., Amiri-Yekta, A., Li, W., Wu, H., Kherraf, Z.E., Liu, W., Zhang, J., et al. (2020). Homozygous mutations in *SPEF2* induce multiple morphological abnormalities of the sperm flagella and male infertility. J. Med. Genet. *57*, 31–37.
43. Yang, Y., Jiang, C., Zhang, X., Liu, X., Li, J., Qiao, X., Liu, H., and Shen, Y. (2020). Loss-of-function mutation in DNAH8 induces asthenoteratospermia associated with multiple morphological abnormalities of the sperm flagella. Clin. Genet. *98*, 396–401.
44. Pleuger, C., Lehti, M.S., Dunleavy, J.E., Fietz, D., and O'Bryan, M.K. (2020). Haploid male germ cells-the Grand Central Station of protein transport. Hum. Reprod. Update *26*, 474–500.
45. Kierszenbaum, A.L. (2002). Intramanchette transport (IMT): managing the making of the spermatid head, centrosome, and tail. Mol. Reprod. Dev. *63*, 1–4.
46. Taschner, M., and Lorentzen, E. (2016). The Intraflagellar Transport Machinery. Cold Spring Harb. Perspect. Biol. *8*, a028092.
47. Lechtreck, K.F. (2015). IFT-Cargo Interactions and Protein Transport in Cilia. Trends Biochem. Sci. *40*, 765–778.
48. Tsurumi, Y., Hamada, Y., Katoh, Y., and Nakayama, K. (2019). Interactions of the dynein-2 intermediate chain WDR34 with the light chains are required for ciliary retrograde protein trafficking. Mol. Biol. Cell *30*, 658–670.
49. Nakayama, K., and Katoh, Y. (2018). Ciliary protein trafficking mediated by IFT and BBSome complexes with the aid of kinesin-2 and dynein-2 motors. J. Biochem. *163*, 155–164.
50. Lehti, M.S., Zhang, F.P., Kotaja, N., and Sironen, A. (2017). SPEF2 functions in microtubule-mediated transport in elongating spermatids to ensure proper male germ cell differentiation. Development *144*, 2683–2693.
51. Wambergue, C., Zouari, R., Fourati Ben Mustapha, S., Martinez, G., Devillard, F., Hennebicq, S., Satre, V., Brouillet, S., Halouani, L., Marrakchi, O., et al. (2016). Patients with multiple morphological abnormalities of the sperm flagella due to DNAH1 mutations have a good prognosis following intracytoplasmic sperm injection. Hum. Reprod. *31*, 1164–1172.
52. Sha, Y.W., Xu, X., Mei, L.B., Li, P., Su, Z.Y., He, X.Q., and Li, L. (2017). A homozygous CEP135 mutation is associated with multiple morphological abnormalities of the sperm flagella (MMAF). Gene *633*, 48–53.

The American Journal of Human Genetics, Volume *108*

Supplemental information

Bi-allelic mutations of *DNAH10* cause primary male infertility with asthenoteratozoospermia in humans and mice

Chaofeng Tu, Jiangshan Cong, Qianjun Zhang, Xiaojin He, Rui Zheng, Xiaoxuan Yang, Yang Gao, Huan Wu, Mingrong Lv, Yayun Gu, Shuai Lu, Chunyu Liu, Shixiong Tian, Lanlan Meng, Weili Wang, Chen Tan, Hongchuan Nie, Dongyan Li, Huan Zhang, Fei Gong, Liang Hu, Guangxiu Lu, Wenming Xu, Ge Lin, Feng Zhang, Yunxia Cao, and Yue-Qiu Tan

Supplemental Note: Case Reports

All individuals presented with typical MMAF phenotypes characterized by multiple flagellar malformations, including absent, short, coiled, bent, and/or irregular-caliber flagella. Subjects with evident PCD-related symptoms,[1] such as recurrent airway inflammation, bronchiectasis, and otitis media, were excluded. Individuals presenting with other causes of infertility, such as reproductive malformation, drug use, and exposure to gonadotoxic factors, were also excluded. No abnormalities were detected with regard to somatic chromosomal karyotypes and Y chromosome microdeletions. The study was approved by the ethics committees of all participating institutes. Informed consent was obtained from all participants at the beginning of the study.

Supplemental References

1. Knowles, M.R., Zariwala, M., and Leigh, M. (2016). Primary Ciliary Dyskinesia. Clin. Chest Med. 37, 449-461.

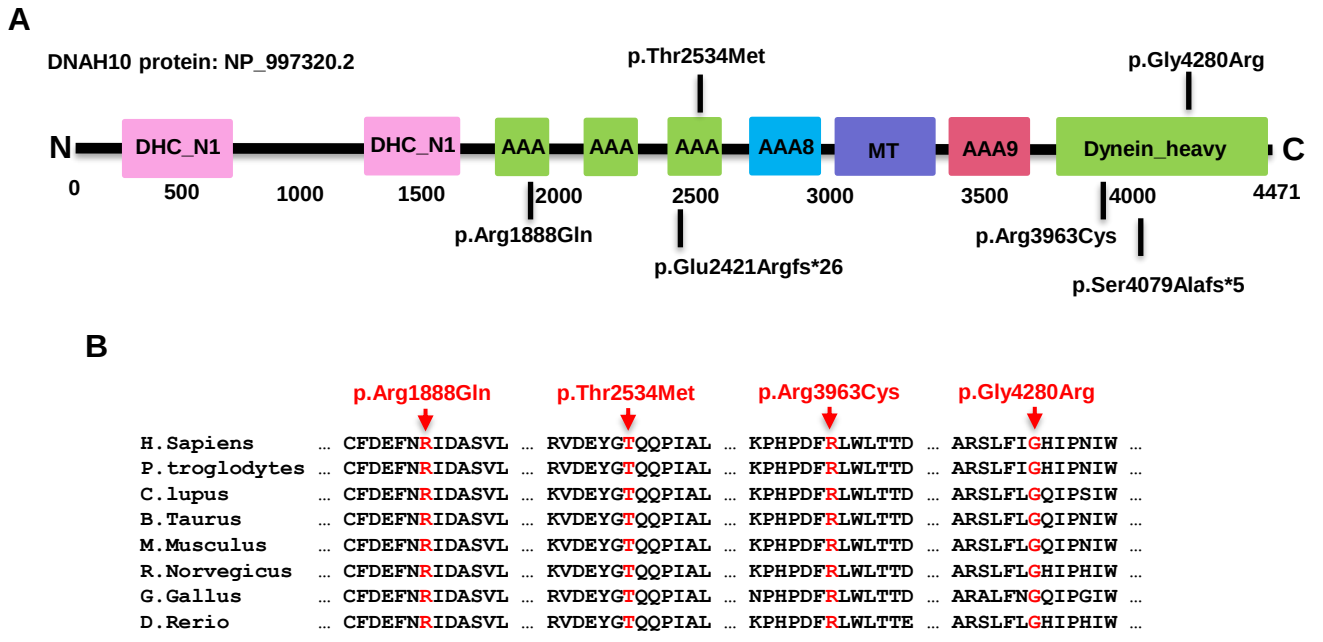

Figure S1. Phylogenetic Conservation of the Mutated Residues in DNAH10 Protein

(A) The positions of six variants in *DNAH10* identified in male cases with asthenoteratozoospermia are shown. Domains/motifs in DNAH10 are indicated in different colored squares according to the NCBI browser.

(B) Sequence alignment shows that the four detected *DNAH10* missense variants are conserved among different species.

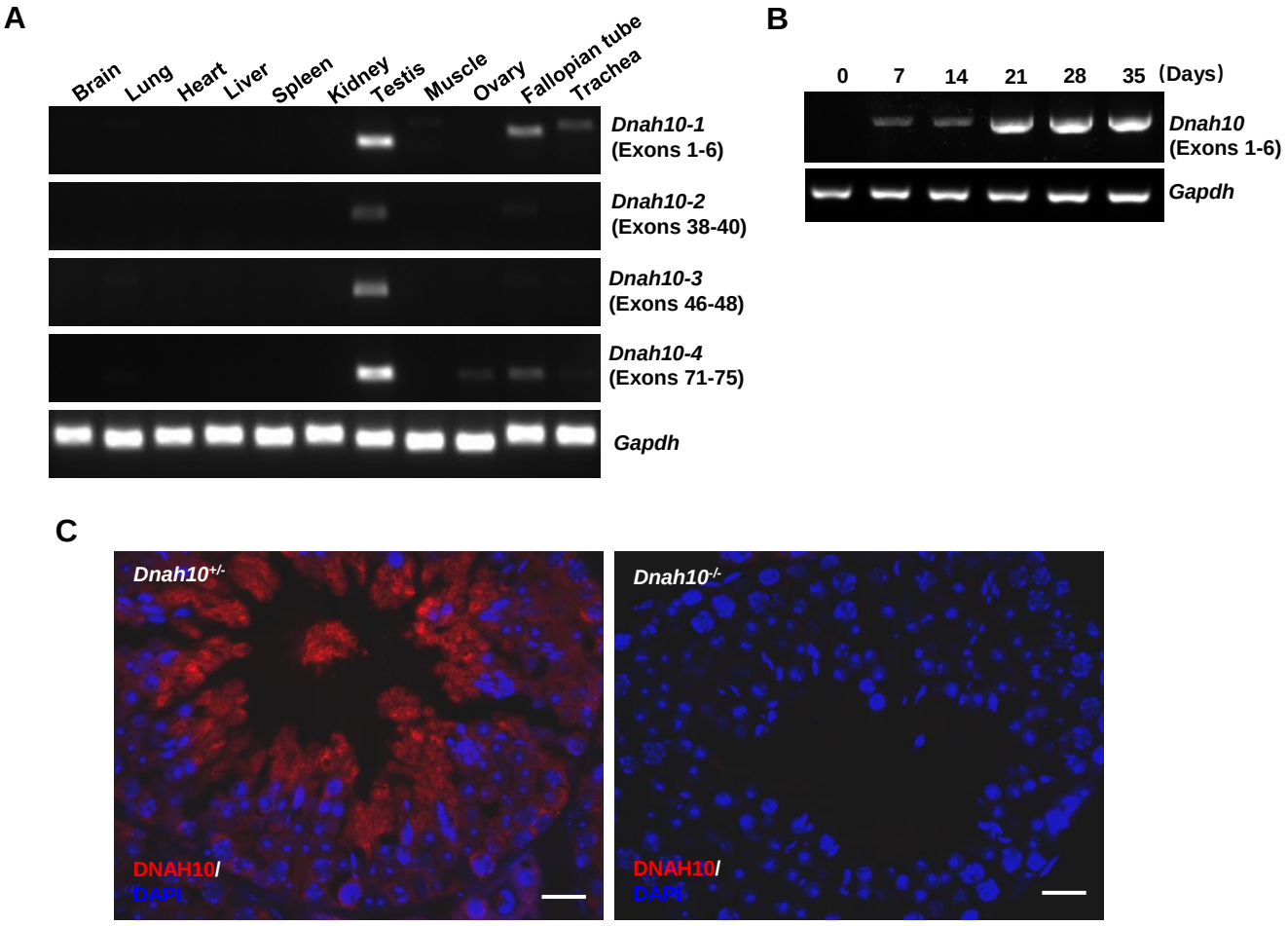

Figure S2. Gene Expression of *Dnah10* in Different Mouse Tissues.

(A) Expressions of *Dnah10* were investigated by RT-PCR in various tissues from adult male mice. *Gapdh* was used as an internal control.

(B) The expression of mouse *Dnah10* mRNA in the testis was highly elevated from postnatal day 21, corresponding to the spermiogenesis stage. Gapdh was as an internal control.

(C) Representative image of testicular tubules stained with anti-DNAH10 antibody and DAPI showing that DNAH10 is localized in the cytoplasm of elongated spermatozoa in the testis from *Dnah10*$^{+/-}$ male mice, but was almost absent in *Dnah10*$^{-/-}$ male mice. Scale bars = 50 μm.

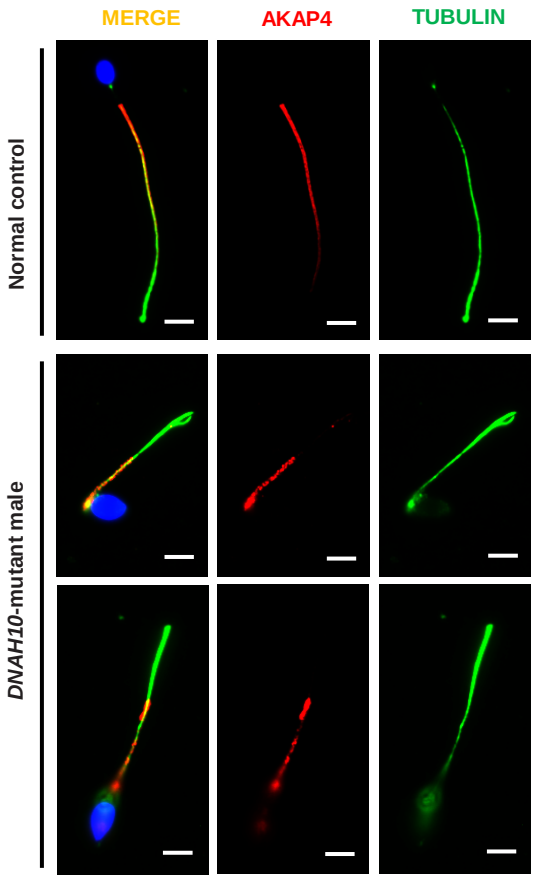

Figure S3. Immunofluorescence Staining of AKAP4 in the Spermatozoa from a Fertile Male Control and Men Harboring Bi-allelic *DNAH10* Variants.

Sperm cells were stained with anti-AKAP4 (red) and anti-α-tubulin (green) antibodies, respectively. DNA was counterstained with DAPI as a marker of the cell nucleus. The AKAP4 signaling in the sperm flagella of individuals with bi-allelic *DNAH10* variants is mislocalized along the sperm tail. Scale bars: 5 µm.

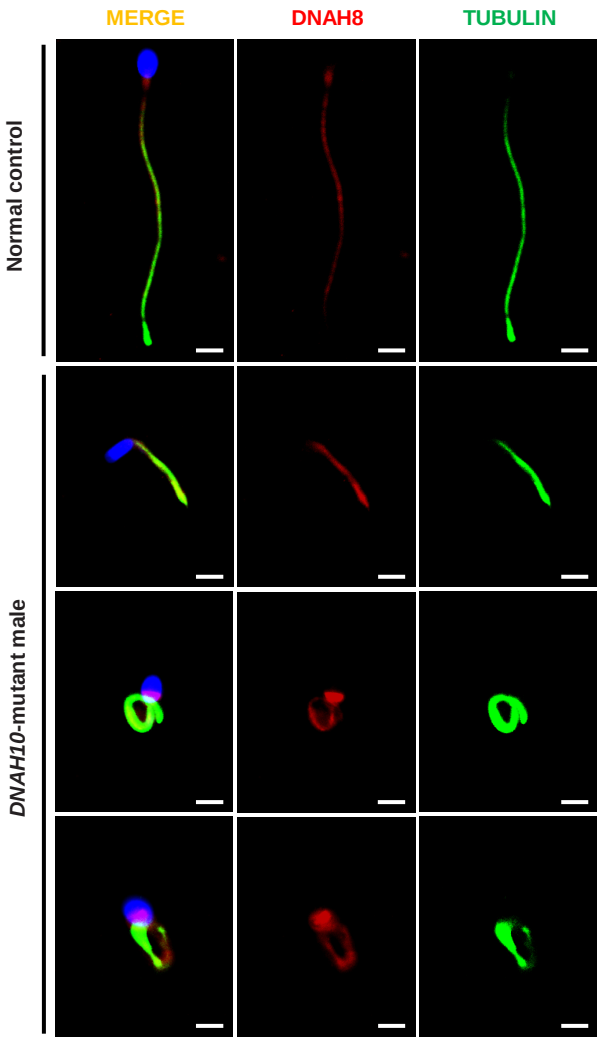

Figure S4. Immunofluorescence Staining of DNAH8 in the Spermatozoa from a Fertile Male Control and Men Harboring Bi-allelic *DNAH10* Variants.

Sperm cells were stained with anti-DNAH8 (red) and anti-α-tubulin (green) antibodies. DNA was counterstained with DAPI as a marker of the cell nucleus. DNAH8 staining is concentrated at the sperm flagella from the normal control and the signal in the *DNAH10*-mutant group is comparable with that of controls. Scale bars: 5 µm.

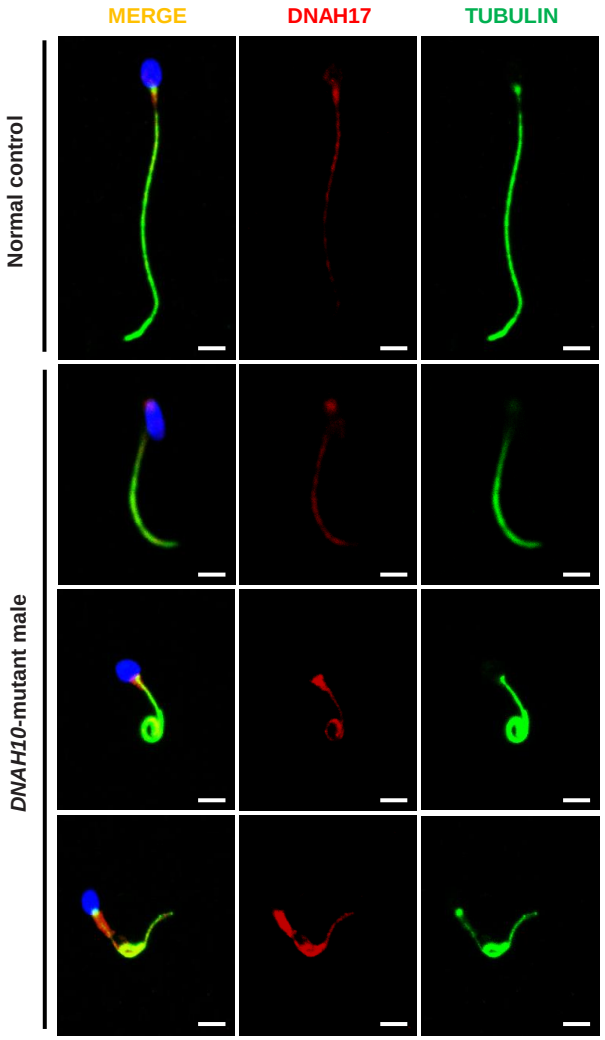

Figure S5. Immunofluorescence Staining of DNAH17 in the Spermatozoa from a Fertile Male Control and Men Harboring Bi-allelic *DNAH10* Variants.

Sperm cells were stained with anti-DNAH17 (red) and anti-α-tubulin (green) antibodies. DNA was counterstained with DAPI as a marker of the cell nucleus. DNAH17 staining is concentrated at the sperm flagella from the normal control and the signal in the *DNAH10*-mutant group is comparable with that of controls. Scale bars: 5 μm.

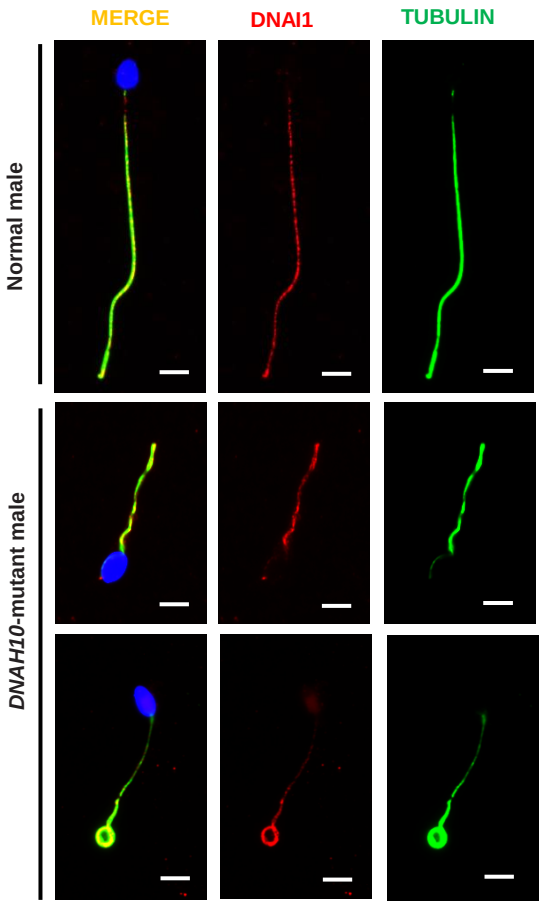

Figure S6. Immunofluorescence Staining of DNAI1 in the Spermatozoa from a Fertile Male Control and Men Harboring Bi-allelic *DNAH10* Variants.

Sperm cells were stained with anti-DNAI1 (red) and anti-α-tubulin (green) antibodies. DNA was counterstained with DAPI as a marker of the cell nucleus. DNAI1 staining is concentrated at the sperm flagella from the normal control and the signal in the *DNAH10*-mutant group is comparable with that of controls. Scale bars: 5 μm.

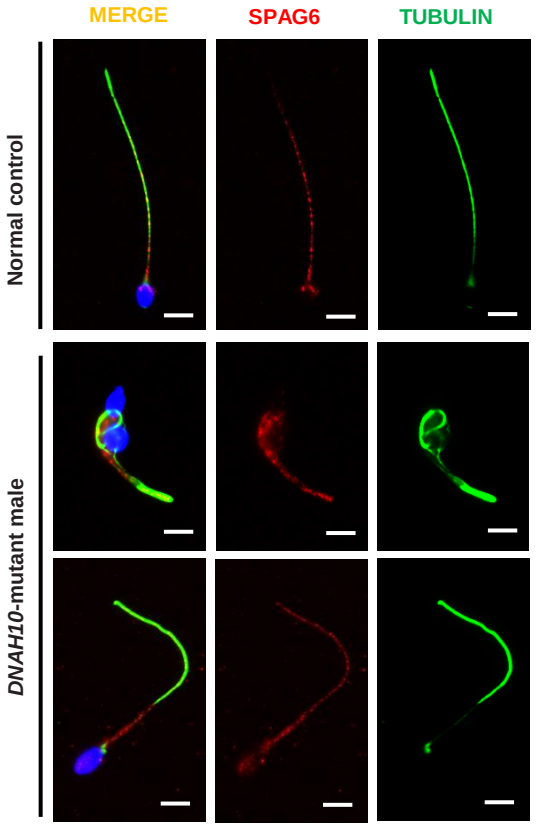

Figure S7. Immunofluorescence Staining of SPAG6 in the Spermatozoa from a Fertile Male Control and Men Harboring Bi-allelic *DNAH10* Variants.

Sperm cells were stained with anti-SPAG6 (red) and anti-α-tubulin (green) antibodies. DNA was counterstained with DAPI as a marker of the cell nucleus. The signal in the *DNAH10*-mutant group is comparable with that of controls, suggesting that central pair was not directly affected by bi-allelic *DNAH10* Variant. Scale bars: 5 μm.

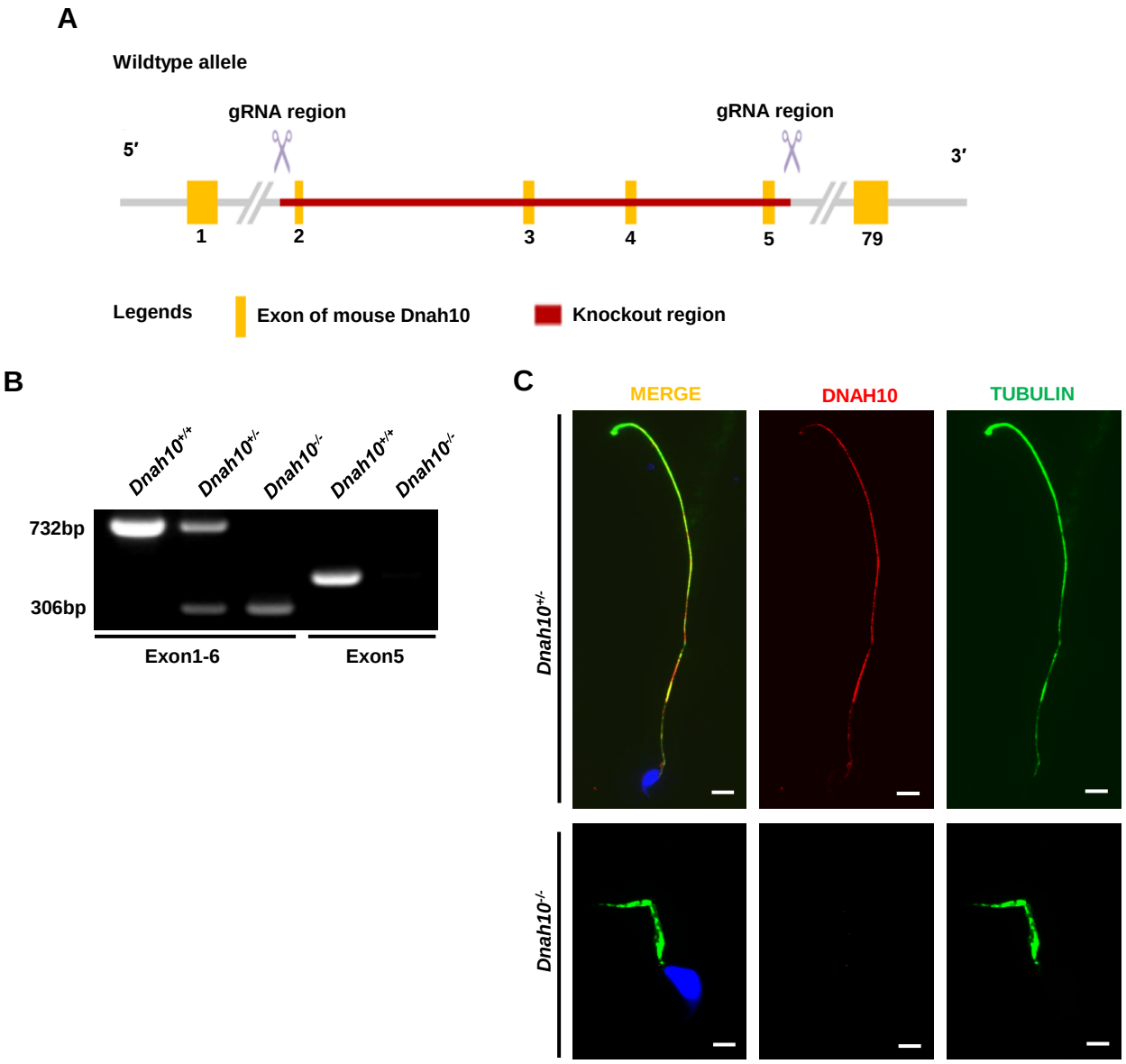

Figure S8. Schematic Illustration of the Targeting Strategy for Generating *Dnah10*$^{-/-}$ Mice

(A) The *Dnah10* knockout strategy in mice. The gRNAs were targeted in exons 2 and 5 of mouse *Dnah10* to delete the partial coding region.

(B) RT-PCR of mRNA isolated from *Dnah10*$^{+/+}$, *Dnah10*$^{+/-}$ and *Dnah10*$^{-/-}$ male mice testes indicated the presence of a truncated transcript in *Dnah10*$^{-/-}$ male mice testes using the *Dnah10* primers which located exon 1 to exon 6 and exon 5, respectively.

(C) DNAH10 (red, specifically binding human amino acids 3561-3700) localized at the entire flagella in the sperm of *Dnah10*$^{+/-}$ male mice. In contrast, DNAH10 staining was absent in the sperm of *Dnah10*$^{-/-}$ male mice. Tubulin indicated the flagella (green), and the nuclei of spermatozoa were counterstained with DAPI (blue). Scale bars = 10 mm.

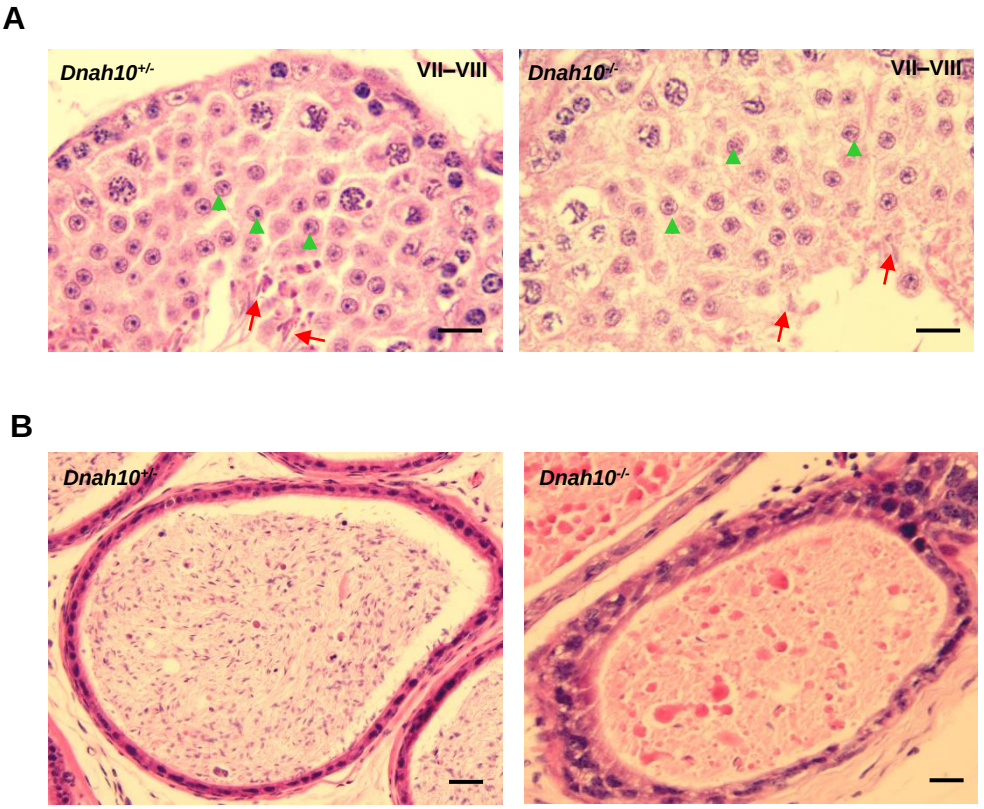

Figure S9. Histological Examinations of Testes and Epididymides from *Dnah10*$^{+/-}$ and *Dnah10*$^{-/-}$ Male Mice

(A) H&E staining of testicular tissues in *Dnah10*$^{-/-}$ male mice and *Dnah10*$^{+/-}$ male mice at 2-month-old. In stage VII–VIII seminiferous tubules from *Dnah10*$^{-/-}$ male mice, normal round spermatids (green, arrowheads) were observed, but the morphology of elongated tails (red arrows) were abnormal. Scale bars = 20 μm.

(B) H&E staining of testicular epididymal sections in *Dnah10*$^{-/-}$ male mice and *Dnah10*$^{+/-}$ male mice at 2-month-old. Compared with *Dnah10*$^{+/-}$ male mice, sperm counts were obviously decreased in the epididymis from *Dnah10*$^{-/-}$ male mice. Scale bars = 20 μm.

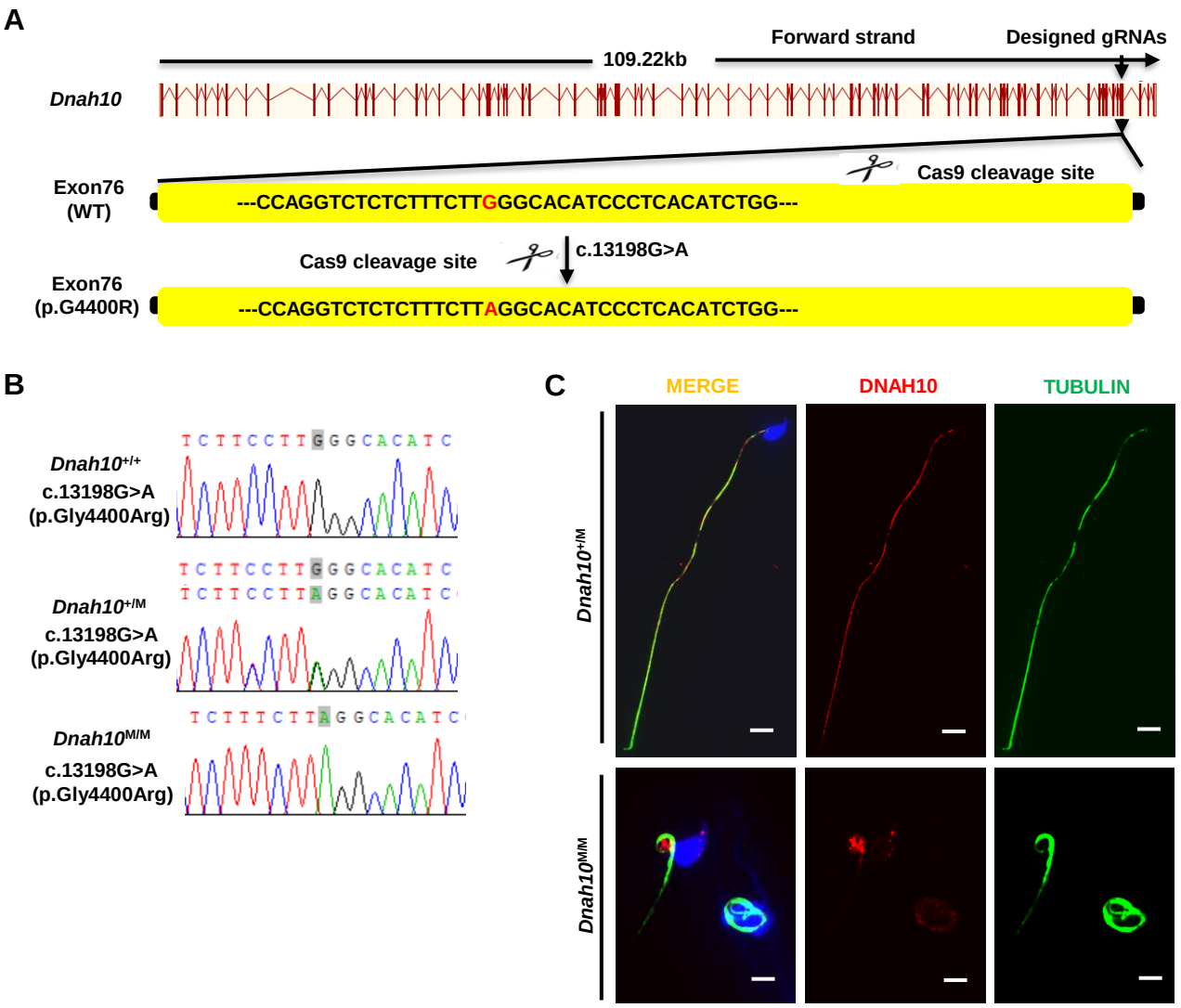

Figure S10. Schematic Illustration of the Targeting Strategy for Generating *Dnah10*$^{M/M}$ Mice

(A) Schematic illustrating construction of the knockin mouse model (*Dnah10*$^{M/M}$). A gRNA was designed targeting exon 76 of *Dnah10*. The mutated nucleotides in mice (c.13198G>A) equivalent to that in *DNAH10*-mutant patient T012 II-2 (c.12838G>A) are written in red.

(B) Sanger sequencing showing the c.13198G>A mutation heterozygous in *Dnah10*$^{+/M}$ and homozygous in *Dnah10*$^{M/M}$ mice.

(C) DNAH10 (red) localized at the entire flagella in the sperm of *Dnah10*$^{+/M}$ male mice. In contrast, DNAH10 staining was reduced in the sperm of *Dnah10*$^{M/M}$ male mice. Tubulin indicated the flagella (green), and the nuclei of spermatozoa were counterstained with DAPI (blue). Scale bars = 10 mm.

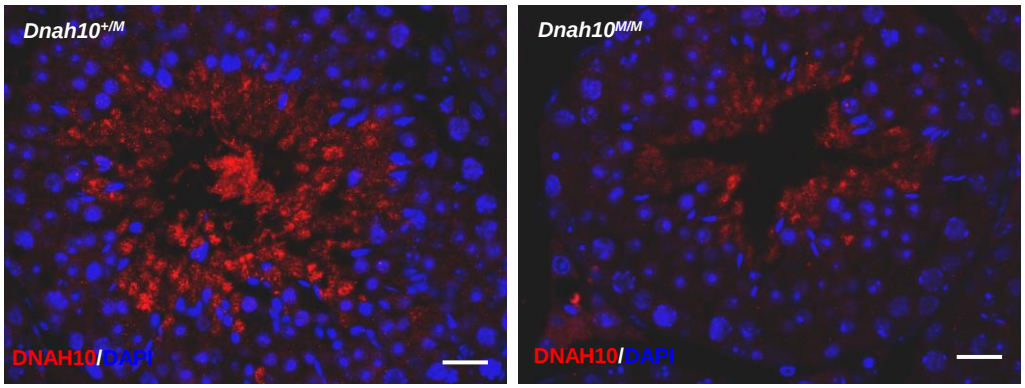

Figure S11. Immunostaining of *Dnah10* in testis from *Dnah10*$^{M/M}$ male mice.

Representative image of testicular tubules stained with anti-DNAH10 antibody and DAPI showing that DNAH10 is localized in the cytoplasm of elongated spermatozoa in the testis from *Dnah10*$^{+/M}$ male mice, but was reduced in *Dnah10*$^{M/M}$ male mice. Scale bars = 50 μm.

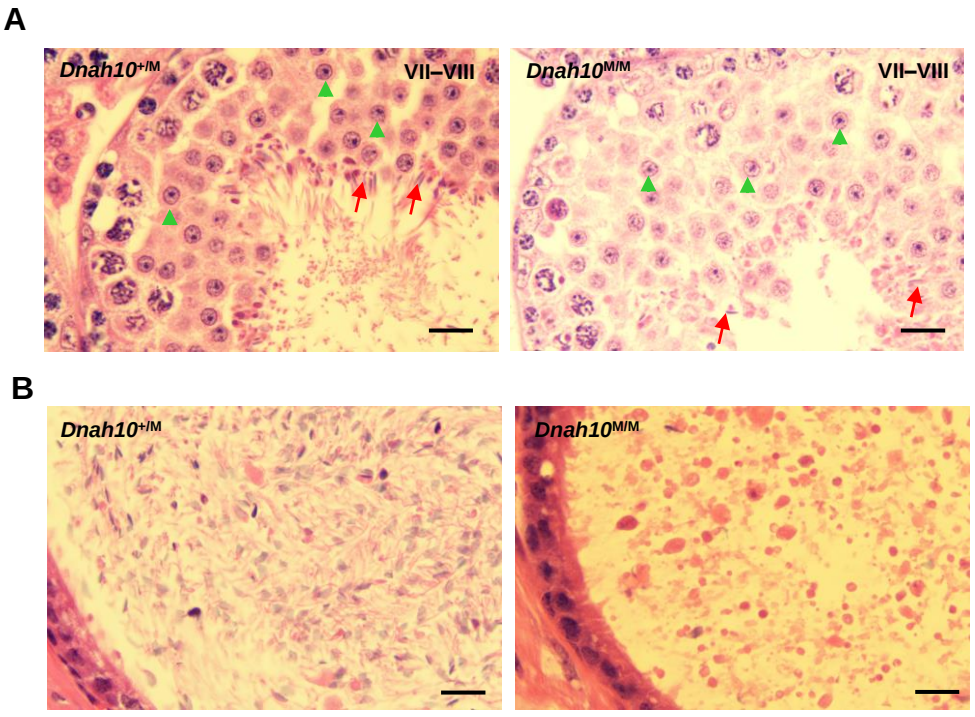

Figure S12. Histological Examinations of Testes and Epididymides from *Dnah10*$^{+/M}$ and *Dnah10*$^{M/M}$ Male Mice

(A) H&E staining of testicular tissues in *Dnah10*$^{M/M}$ male mice and *Dnah10*$^{+/M}$ male mice at 7 weeks old. In stage VII–VIII seminiferous tubules from *Dnah10*$^{M/M}$ male mice, normal round spermatids (green, arrowheads) were observed, but the morphology of elongated tails (red arrows) were abnormal. Scale bars = 20 μm.

(B) H&E staining of epididymal sections in *Dnah10*$^{M/M}$ male mice and *Dnah10*$^{+/M}$ male mice at 7 weeks old. Compared with *Dnah10*$^{+/M}$ male mice, sperm counts were obviously decreased in the epididymis from *Dnah10*$^{M/M}$ male mice. Scale bars = 20 μm.

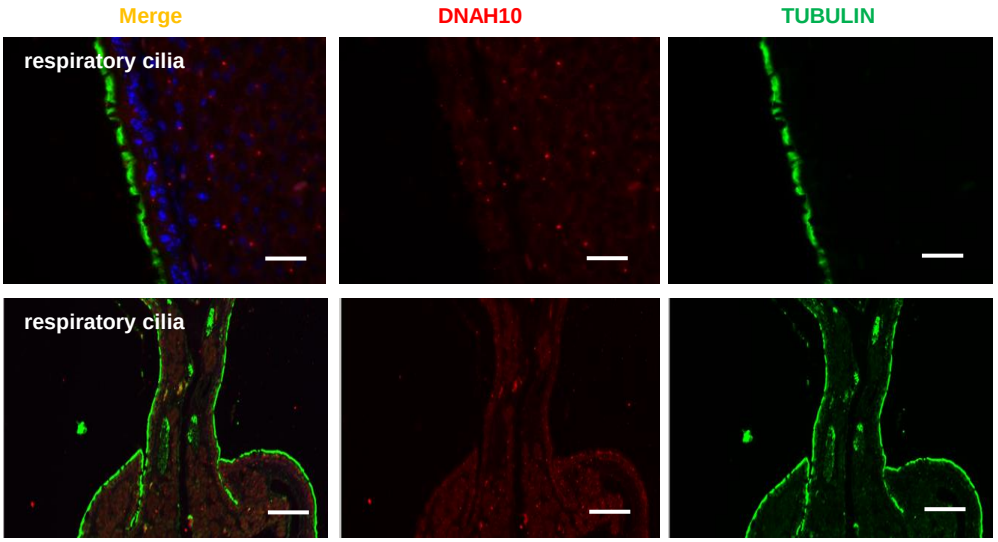

Figure S13. Immunofluorescence Staining of DNAH10 in the Respiratory Cilia from a Fertile Male Control.

Respiratory cilia cells were stained with anti-DNAH10 (red) and anti-α-tubulin (green) antibodies. DNA was counterstained with DAPI as a marker of the cell nucleus. DNAH10 staining using the antibody recognizing the C-terminus of DNAH10 (amino acids 3561-3700) is not detectable at the respiratory cilia. Scale bars = 20 μm.

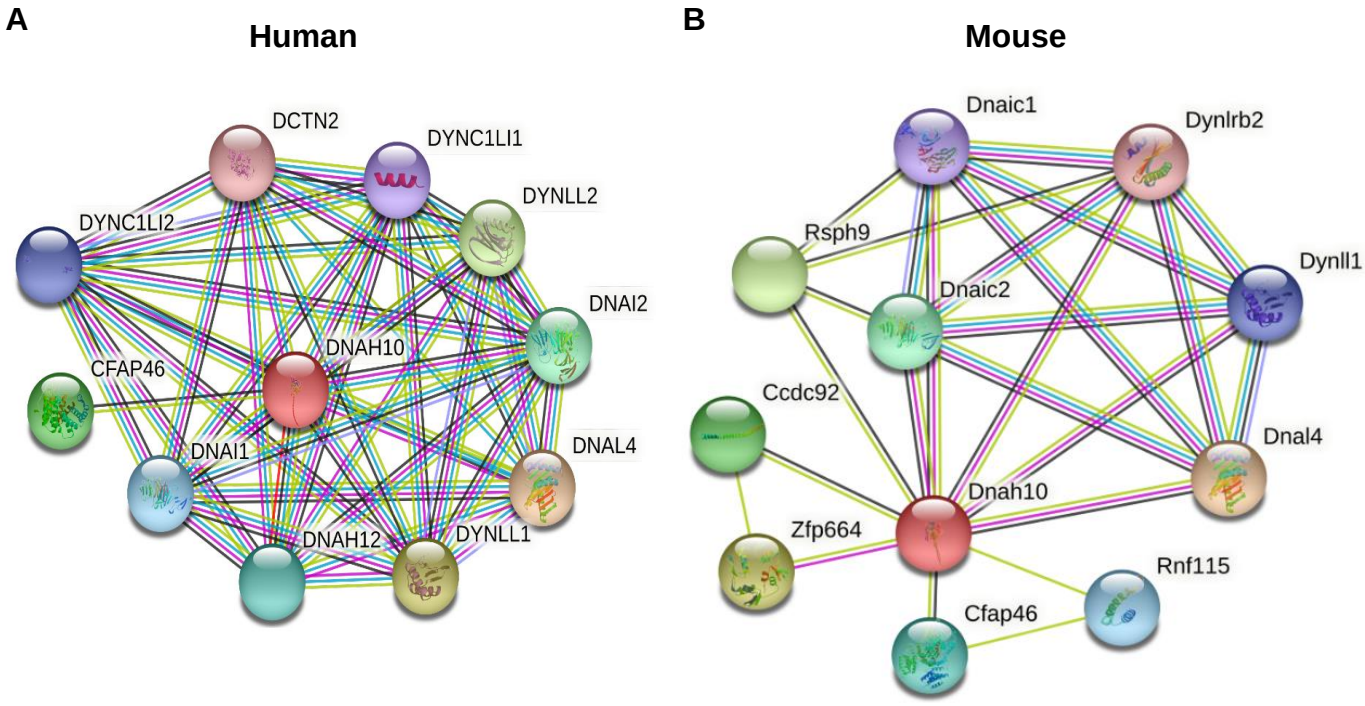

Figure S14. The Protein-Protein Interactions for DNAH10/Dnah10 Predicted by STRING.

The protein interaction networks were predicted using *in silico* software String for human and mouse DNAH10/Dnah10 proteins, respectively. The direct interaction was predicted between human DNAH10 and DYNLL2, DYNC1LI2 and DYNC1LI2, but no direct interaction was shown between mouse Dnah10 and Dynll2, Dync1li2 and Dync1li2. The yellow lines suggest the interactions using text mining, and black lines indicate the identification of co-expression.

Table S1. Primers Used for Verification of *DNAH10* Variants

Primer name	F/R	Primer Sequence (5' to 3')	Annealing Temperature (℃)
DNAH10 (c.G12838A)	F1	GGATGACGAAGTCTCTGGCTG	57
	R1	CTAGGCTGACACCTGAATCGG	
DNAH10 (c.7601C>T)	F2	AAACTGAAACCGAGGTGCCC	58
	R2	CTTGGGTCAACTTCATTGCGG	
DNAH10 (c.5663G>A)	F3	GGCTGGTCACCTGCTT	51
	R3	CCACGCCCATTCATAAC	
DNAH10 (c.11887C>T)	F4	CCCGACTTCCTGGTG	48
	R4	AGCGGCTCCCTCTAA	
DNAH10 (c.7260dup)	F5	CATCTGTCCAGTGATGAG	55
	R5	GCATCTCATCTGCCTGTGG	
DNAH10 (c.12235del)	F6	GATTGGCTGGAACGTGTACTA	56
	R6	GGAATTGATGTCACTGCC	

Abbreviation: F, forward primers; R, reverse primers.

Table S2. Primers Used for Mouse *Dnah10* Genotyping

Primer name	F/R	Primer Sequence (5' to 3')	Annealing Temperature (℃)	Length (bp)
Dnah10-KO	F1	GGTGCCTTCACTCTGTAAGTGTC	60	791
	R1	GCTGTCTGTTACACTGATGGATG		
Dnah10-KO	F2	GGTGCCTTCACTCTGTAAGTGTC	60	622
	R2	GCTTCATTTCCTCCAGACACCC		
Dnah10-KI	F3	CTGGTGGTTGGAGGTAGCTTT	58	342
	R3	CTGGAAGAAATCATCATAGGAG		

Abbreviation: F, forward primers; R, reverse primers; KO, knockout. KI, knockin.

Table S3. Primers Used for RT-PCR Assays

Primer name	F/R	Primer Sequence (5' to 3')	Annealing Temperature (℃)	Length (bp)
Dnah10-1 (Exons 1-6)	F1	AACCTCACCAACCCTATGCT	55	732
	R1	ATCGCGGATCAGTTGGACG		
Dnah10-KO (Exon 4-7)	F2	TTCAAAAGACGCCATCCCAGAA	57	448
	R2	GATCACGCACTGCTCCAAAT		
Dnah10-2 (Exon 38-40)	F	TTATGTGCTCCTGCCAGTCC	57	371
	R	TGTTGTCGTCCATCACGGAG		
Dnah10-3 (Exon 46-48)	F	GAACATGCCAAAGGTGGATGAG	57	237
	R	TTCAGGGACTCCTCCGATGG		
Dnah10-4 (Exons 71-75)	F	TGACTTCCAGGTCTGTATGGAAAT	56	422
	R	TGCTGGACTCCCCTGTCTG		
Gapdh (RT-PCR in Mice)	F	GGTGAAGGTCGGTGTGAACG	57	233
	R	CTCGCTCCTGGAAGATGGTG		

Abbreviation: F, forward primers; R, reverse primers; KO, knockout.

Table S4. Semen Routine Parameters and Sperm Flagellar Morphology in Men Harboring Bi-allelic *DNAH10* Variants

Subject	T012 II-2	T089 II-1	H049 II-2	NK067 II-1	NK067 II-2	Reference Limits
Semen Parameter						
Semen volume (mL)	6.7	3.3	2.0	3.7	2.6	>1.5[a]
Sperm concentration (10^6/mL)	1.6*	0.5*	6.6*	71.2	72.6	>15.0[a]
Motility (%)	0*	0*	9.2*	10.3*	11.8*	>40.0[a]
Progressive motility (%)	0*	0*	1.7*	1.9*	2.4*	>32.0[a]
Sperm Flagella Morphology						
Absent flagella (%)	3.6	12.0*	11.8*	24.5*	4.5	<5.0[b]
Short flagella (%)	29.0*	21.0*	8.8*	15.6*	9.1*	<1.0[b]
Coiled flagella (%)	38.5*	45.0*	41.2*	38.1*	58.3*	<17.0[b]
Angulation (%)	7.5	3.5	30.9*	6.1	3.8	<13.0[b]
Irregular caliber (%)	8.0*	5.5*	2.9*	4.1*	2.3*	<2.0[b]

[a]Reference limits according to the WHO standards.[43]

[b]Reference limits according to the distribution range of morphologically normal spermatozoa observed in 926 fertile individuals.[44]

*Abnormal value

Table S5. Rates of Ultrastructural Abnormalities in the Spermatozoa from Men Harboring Bi-allelic *DNAH10* Variants.

Subject	Control [a] (n=45)	T012 II-2 (n=30)	NK067 II-1 (n=25)	NK067 II-2 (n=45)
Missing IDA	0 (0%)	15 (50.0%)	18 (72.0%)	31 (68.9%)
Missing CP	1 (2.2%)	1 (3.3%)	0 (0%)	2 (4.4%)
Missing MT	4 (8.9%)	6 (20.0%)	0 (0%)	1 (2.2%)
Global disorganization	1 (2.2%)	3 (10.0%)	0 (0%)	4 (8.9%)

[a] Values represent the mean of three normal males; n, number of cross sections for analysis.

Abbreviations: IDA, inner dynein arms; CP, central pair of microtubules; MT, peripheral microtubule doublet.

Table S6. Sperm Morphology in *Dnah10*-Mutated Male Mice [a]

	***Dnah10*$^{+/+}$**	***Dnah10*$^{-/-}$**	***Dnah10*$^{M/M}$**
Sperm Morphology [b]			
Absent flagella (%)	3.5 ± 0.4	13.5 ± 0.6	10.5 ± 0.5
Short flagella (%)	0.3 ±0.9	22.3 ±0.5	25.3 ±0.7
Coiled flagella (%)	2.1 ± 0.5	40.6 ± 0.7	37.6 ± 0.5
Irregular caliber (%)	0.9 ± 1.1	12.9 ± 0.9	16.9 ± 0.6
Bent flagella (%)	1.7 ± 0.7	10.7 ± 0.5	9.7 ± 0.7

a Values represent the mean (range).

b Per single epididymis.

Table S7. Clinical Outcomes of ICSI Cycles Using the Spermatozoa from Men Harboring Bi-allelic *DNAH10* Variants

Subject	T012 II-2	H049 II-2	NK067 II-2
Male age (year)	30	37	38
Female age (year)	30	29	34
Number of ICSI cycles	1	1	1
Number of oocytes injected	11	6	15
Number (and rate) of fertilized oocytes	9(82%)	5(83%)	12(80%)
Number (and rate) of cleavage embryos	9(100%)	5(100%)	12(100%)
Number (and rate) of 8-cells	6(66%)	4(80%)	10(83%)
Number (and rate) of blastocysts	6(66%)	3(60%)	9(75%)
Number of transfer cycles	1	1	1
Number of embryos transferred per cycle	2	2	2
Implantation rate	50%	0	50%
Clinical pregnancy rate	100%	NA	100%
Miscarriage rate	NA	NA	NA

NA, not available.